ELECTRON TRANSFER IN ELECTROCHEMICAL ENVIRONMENT

By

A. Vallan Bruno Cruz

The Institute of Mathematical Sciences, Chennai.

A thesis submitted to the
Board of Studies in Physical Sciences

In partial fulfillment of the requirements
For the Degree of

DOCTOR OF PHILOSOPHY

of

HOMI BHABHA NATIONAL INSTITUTE

December 2010

Homi Bhabha National Institute

Recommendations of the Viva Voce Board

As members of the Viva Voce Board, we recommend that the dissertation prepared by **A. Vallan Bruno Cruz** entitled "Electron Transfer in Electrochemical Environment" may be accepted as fulfilling the dissertation requirement for the Degree of Doctor of Philosophy.

---------- **Date :**
Chairman :

---------- **Date :**
Convener :

---------- **Date :**
Member :

---------- **Date :**
Member :

---------- **Date :**
Member :

---------- **Date :**
Member :

Final approval and acceptance of this dissertation is contingent upon the candidate's submission of the final copies of the dissertation to HBNI.

I hereby certify that I have read this dissertation prepared under my direction and recommend that it may be accepted as fulfilling the dissertation requirement.

---------- **Date :**
Guide : A. K. Mishra

DECLARATION

I, hereby declare that the investigation presented in the thesis has been carried out by me. Whenever contributions of others are involved, every effort is made to indicate this clearly, with due reference to the literature and acknowledgement of colloborative research and discussions. The work is original and the work has not been submitted earlier as a whole or in part for a degree/diploma at this or any other Institution or University.

A. Vallan Bruno Cruz

ACKNOWLEDGEMENTS

This thesis would not have been possible if not for the meticulous efforts and timely suggestions provided by my Advisor Prof. A. K. Mishra. He has made available his support in numerous ways. I benefitted a lot from his physcial insight and I am thankful for his infinite patience. I would also like to express my gratitude towards Prof. G. I. Menon and Prof. S. R. Hassan for the providing timely assistance thoroughout my stay in IMSc. I would be regarded ungrateful if I do not mention the name of Prof. G. Baskaran. He has been a motivating force for not only me but to all students in IMSc. The time spent with him in discussion were fruitful and illuminating.

My friends in IMSc require a special mention since their continued presence distracted me from completeing my thesis years ago but they also made my stay in IMSc a pleasant one.

I consider myself fortunate to be associated with Prof. W. Schmickler. Discussion session with him were always a novel experience and a fruitful and enjoyable moment.

Abstract

Transport of electrons in molecular junction devices is one of the important problem in the field of molecular electronics and nanoscale devices. Though in the past years formalisms have been successfully developed to account for tunneling associated with energy gap between Fermi-levels and molecular levels, coherent and incoherent tunnelings and inelastic tunneling spectroscopy. A successful picture for general understanding of orientational and vibrational effects on molecular junction devices, typically as encountered in electrochemical environment, is yet to be fully perceived. Additionally, since in electrochemical environment the bias and electrochemical potential of the wire can be varied independently, a thorough understanding of the electron transfer process in such a system can help in predicting behaviours like current rectification, negative differential resistance etc. Experimentally this is easily realised by operating in electrolyte and to control the potential of two electrodes with respect to a reference electrode in the electrolyte. This is desirable in lieu of downscaling of electronic components since the applied gate voltage falls across the double layers of the electrode-electrolyte interfaces which are a few angstroms in extent.

Initially works on electron transfer were aimed at DBA complexes. The situation of electron transfer between reservoirs connected by a molecular bridge was investigated by Ratner and co-workers. Formal expressions were obtained by Caroli and co-workers which were later re-derived by several others in different context. In this thesis considerable attention will be paid to the case of a molecular bridge containing a redox center. The presence of redox complicates the analysis as the redox couple can interact with the solvent whose fluctuations will have enhanced effect on the current. This situation is studied in detailed in this thesis. Modelling the bridge wire by a tight-binding hamiltonian and the interaction of the redox with the solvent polarization modes as linear coupling, an explict expression for quantum conductance (within the wide-band approximation) is obtained. The thermal averages over various polarization modes is performed numerically. Depending upon the strength of interaction between neighbouring atoms, various intereating current-voltage responses are seen. The considered system is shown to

exhibit certain desirable feature of electronic circuits such as rectification, negative differential resistance, step behaviour (extended current voltage plateaus) etc.

Though the traditional view of electron transport theories in electrochemical environment is to consider a transfer between two reservoirs or between DBA complexes wherein the donor and acceptor states are in discrete energies, we present our result in this thesis for the electron transfer rate from a redox to a reservoir. This problem demands attention since while the reservoir normally has a continuum of states while the redox which has single energy level but is dependent on the fluctuation of the solvent, that is, the polarization mode of the solvent. Hence the total electron transfer rate is determined by the competition between the resonance tunneling of the electron and the solvation of the redox. Assuming the solvent exits in a thermal equilibrium independently, the transfer rate was studied while varying some of the important parameters like the re-organisation energy, the relative position between the bridge and the Fermi-level etc.

In actual experiment, the molecular wire is connected to an electrode by means of a contact group. In general, the contact group is a species different from the atoms of the molecular bridge and which chemisorbs well with the electrode. In this thesis, electron transfer through such a chemically modified electrode is presented. Further, to correspond better with actual experimental setup, the adsorbate is randomly distributed on the electrode surface and it's coverage factor is allowed to vary from zero to 1 this covering all regimes, from lone adsorbate to monolayers. A modified Newns-Anderson Hamiltonian is employed to model the system and the current is calculated within the linear response regime. The randomness in the adsorbate distribution is handled using CPA. The DOS is analysed for different regimes of strong and weak coupling as well as lone and monolayer coverage regimes. The current-potential profiles are similary plotted for various limiting regimes. We recover the Marcus inverted regime in the low coverage case and also a direct heterogenous electron transfer in the high coverage regime when the coupling is strong. A saddle point behaviour is observed in the low coverage regime with weak coupling.

List of publications/preprints

1. A. Vallan Bruno Cruz, A. K. Mishra and W. Schmickler. “Electron tunneling between two electrodes mediated by a molecular wire containing a redox center ,” [arXiv:cond-mat.mes-hall/0912.1165], (to appear in Chemical Physics, doi:10.1016/j.chemphys.2010.01.009)

2. A. Vallan Bruno Cruz, A. K. Mishra and W. Schmickler, “Electron Transfer rate between a electrode and a bridged redox ," [arXiv:cond-mat.mes-hall/0912.3083]

3. A. Vallan Bruno Cruz, A. K. Mishra and W. Schmickler, “Electron Transfer Reaction Through an Adsorbed Layer," [arXiv:cond-mat.mes-hall/0912.2856]

Contents

List of Figures

List of Tables

Chapter 1

Introduction

In 1965, Gordon Moore, proposed his famous 'Moore's Law' [2] which states that there would be a doubling of devices per chip every 24 months and has been seen to hold good for the past 40 years. Clearly such a scaling of the components is expected to lead to a region where quantum effects become predominant. This has lead to an increased interest in the field of nanotechnology both at a formalism level as well as from a technological point of view. The active research in formalisms is more geared towards a better understanding of the transport phenomena involved as well as predicting the behaviour of envisioned devices under given set of conditions. The recent focus at this front has moved from understanding simple tunneling near Fermi surface and energy bands to including effects of electronic and vibrational degrees of freedom. While the engineering aspect is more towards device design, which in turn basically involves around manipulating materials at atomic length scales. The success in the latter is basically due to the developments in STM, AFM and in general MJT's [3, 4, 5, 6, 7, 8, 9, 10, 11, 12].

There has always been a need for high speed computing along with low consumption of power and compactness of computing devices. Present day computing is dominated by semiconductors which faces certain setback factors in view of the downsizing for devices. The chief among them are scaling at atomic dimension, gate oxide thickness, power consumption due to leakage current, quantum tunneling etc[13]. All the above mentioned factors have made molecules as a potential candidate for future computing

devices. Molecules on the contrary have certain desired features. Molecules within a typical size of 1 to 100 nm can have a variety of structures. Isomers of the same molecular family can have different electronic properties, a behaviour highly desired for switching operations at single molecule level. By suitable choice of composition, it is possible to vary the transport properties of a molecule extensively.

1.1 Electron Transfer Theories

In Semiconductors and metals the electron transport can be understood from a Ohmic picture, that is, resistance is proportional to length of wires, for a fixed cross-section of wire. Such a picture fails for molecular conduction due to the localized electronic states. A particular interesting case is that of conduction through a DBA-molecule (Donor-Bridge-Acceptor), which has been well studied in literature both experimentally as well as theoretically. In DBA molecules, the donor and acceptor sites are part of the same molecule and correspondingly three different mechanisms are possible for electron transfer. One is the thermal excitation from donor to acceptor which is incoherent and diffusive, while the other two mechanism are electron super-exchange (electrons tunnel from one electrode to the donor then to the acceptor and finally to the other electrode), and hole exchange (where the electron first leaves the molecular level creating a hole which is then followed by refilling)[14, 9]. The latter two mechanisms are coherent in nature. It should be noted that the general observed I-V charactersitics implies a coherent transport of electrons. The conduction, under certain conditions, can be made to vary with the sign of applied voltage, thus leading to rectification [15] . The chief factor in determining the conduction behaviour of DBA molecule is the rate of electron transfer from donor to acceptor. This prompts one to study conduction properties interms of electron transfer rate between donor and acceptor species.

The most successful of electron transfer theories is one due to Marcus [16] , where the transfer rate for non-adiabatic case is calculated.

$$\kappa_{et} = \frac{2\pi}{\hbar}|V_{DA}|^2 \rho_{FCWD} \tag{1.1}$$

where ρ_{FCWD} is the Franck-Condon weighted density of states and V_{DA} is the coupling between donor and acceptor electronic states. Further, if E_{DA} is the difference in electronic energy between the donor and acceptor and λ the solvent re-organisation energy, it was shown by Marcus that the above rate reduces in classical limit to an expression which is now the well-known Marcus expression for electron transfer rate

$$\kappa_{et} = \frac{2\pi}{\hbar}|V_{DA}|^2 \frac{e^{-(\lambda + E_{DA})^2/4\lambda k_B T}}{\sqrt{4\pi\lambda k_B T}} \tag{1.2}$$

For coherent transport, an approximate expression was derived by A.Nitzan[17] relating the electron transfer rate to the conductance. He considered N identical segments in which only the first (1) and last (N) bridges sites were coupled to the donor and acceptor. The donor and acceptor species are assumed to be chemisorbed on the electrodes. Let Γ_D and Γ_A be the imaginary part of their self-energies arising due to their coupling with electrodes. Under this set of assumptions, for low bias, conductance g was found to have the form

$$g \approx \frac{8e^2}{\pi^2 \Gamma_D^L \Gamma_A^R \rho_{FCWD}} \kappa_{et} \tag{1.3}$$

Though the above formula presents a simple correspondence between the two observables, namely the electron transfer rate and the conduction, certain factors needs to be taken into consideration in a general scenario. Thermal activation can dominate at suitable temperatures leading to dephasing and hence shifting the transport process from coherent regime to incoherent hopping. The above effect will lead to a length dependency in the transport. Since most molecules are highly sensitive to temperature changes, junction heating needs to be addressed. This brings the next important aspect of electron-phonon coupling which is primarily responsible for junction heating. Additionally, stochastic switching involves molecules that have their electronic transport properties strongly dependent on underlying nuclear conformations [18, 19, 20] . This has been proved in an experiment by M. Berthe and co-workers [21] where electron transport takes place only when the bridge is vibrational excited.

Traditional treatment in ET theories heavily relies on Franck-Condon approximation, where the transport is assumed to be independent of the geometry. Evidently there is a breakdown Franck-Condon approximation for conductance in such cases as mentioned above.

1.2 Experimental overview

Conductance measurements serve as a first test for the applicability of the formalisms developed to fabricated devices. The most simplest is to use a scanning tunneling microscope to study the electron transport through individual molecule adsorbed on the surface [22, 23, 24, 25]. Differential conductance can be obtained from such an experiment but the important assumption in such a picture is the applicability of Tersoff-Harmann picture [26]. In Tersoff-Harmann picture, the conductance is proportional to the local density of electronic states of the STM tip and the Fermi energy. This is justified since there exist a large vaccum gap between the molecular end and the STM tip and most of the voltage drop occuring in the gap.

It is possible to measure the conductance properties in the presence of a gate voltage. The above measurements discussed were done in the absence of a reference potential. The application of three terminal junctions has become common from the introduction of CMOS transistors. In molecular electronics proposals have been made to employ the three terminal junctions to change the nature of transport from coherent to hopping transfer [27, 28, 29]. Attempts have been made to incorporate semiconductors in molecular conduction. Most of the experiments on molecular transport employs gold electrode with thiol anchor for the molecular wire. The primary factor for this combination for the interface is that the Fermi energy of gold electrode fall within the HUMO-LUMO gap of most thiol ended molecules. Experiments using semiconductor as the electrode have been performed [30, 31, 32]. The main advantage of using semiconductor for the junction is that, a typical metal-molecule junction suffers for geometric changes which can affect the transport property through the junction, while a in a semiconductor-molecule

junction, such a uncertainty is not present since the is interface formed by two-atoms sharing electron through a covalent bond. Additionally, the band-gap is expected to provide negative differential resistance [33, 34]. Some theoretical studies have also been done for semiconductor-molecule interface[33, 35], most of them focus on the band gap domination of the transport properties.

The traditionally employed three terminal voltage measurements, which forms the basis for switching devices, suffers from a serious drawback. The mode of operation of a switching device is to control to flow of current by a third electrode. Obviously for molecular electronics, this would imply placing the third electrode at a distance of a few angstroms from the desired molecule. This method has serious constructional constraints. Another method would be to employ a large gating voltage to manipulate the energy levels of the molecule which is again not economical, especially in lieu of heat dissipation. An alternate viable solution is to use molecules with redox centers and to control the states of the redox using gating voltage. The presence of third electrode can be avoided by operating the setup in an electrolyte and the reference electrode in the electrolyte can be used as the gate electrode. This is advantageous as the applied voltage falls mainly across the double-layer at the electrode-electrolyte interface. Several groups have reported successful implementation of the above method to control charge transfer in serveral diverse situations like nanojunction [36] , polymer films [37], carbon nanotubes [38, 39], redox molecules [1, 40, 41, 42, 43] etc.

1.3 Preliminary terms and concepts

The transport phenomenon in molecules typically takes place within a few nanometers of length scale and hence it is advantageous to characterise the conduction by using concepts developed for mesoscopic conductors. Obviously the first of these are the length scale which serves to roughly differentiate between the classical and quantum regime [44]. Typically, these length scales are the Fermi wavelength λ_F, the momentum relaxation length L_m and the phase relaxation length L_ϕ. These are throughly discussed by Datta in his well written book on mesoscopic conduction [45].

1.3.1 Fermi Wavelength

At very low temperatures, it is well known that only electron close to the Fermi surface contribute to current. The Fermi wavelength scales as the inverse square root of Fermi energy, $\lambda_F = 2\pi/\sqrt{2mE_F}$. Numerically this is of the order of a few nm. If the transport happens in one dimension, then there exist only one channel, but for two dimensional transport the number of channels or modes available for propagation is determined by the ratio of the band-width W of the wire to the Fermi wavelength $INT(2\lambda_F/W)$, where $INT(x)$ is the largest integer smaller than x. Hence changing the width results in decrease in the number of channels available for electrons to pass and thus leading to a step like increase or decrease of the conductance.

1.3.2 Momentum relaxation length

The momentum relaxation length L_m is the average distance traveled by the electron before losing it's momentum by collison with impurities, defect etc. Numerically this is of the order a few microns. In elastic scattering the momentum changes even though the energy remains conserved and hence elastic scatter contributes to the momentum relaxation length. Thus both elastic scattering and inelastic scattering (i.e. scattering with lattice vibrations, core electrons etc) both contribute to momentum relaxation but electron-electron scattering does not contribute to the above relaxation

1.3.3 Phase relaxation length

This length L_ϕ is defined as the distance traversed before the electron looses information about it's initial phase. Dynamical scatters like phonons, magnetic impurities are

primary factors contributing to phase relaxation. Elastic scattering does not change the phase of electrons while scattering between two conduction electrons can lead to phase changes. At low temperature electron-electron scattering is the primary factor in bringing about phase relaxation.

The above characteristic length scale can be changed by varying certain experimental parameters or by changing the material properties. For example, the phonon excitations can be suppressed by lowering the temperature which in term increases L_m and L_ϕ. Magnetic scattering can be controlled by altering the concentration of the scatters or by using a suppressing magnetic field. Similarly electron-electron interaction is dependent on carrier concentration and band structure. So the transport behaviour can be studied separately by preparing the samples under suitable external control parameters.

Apart from the above mentioned length scale to characterise the transport process, certain additional notions are needed in order to have a clarity in understanding molecular transport phenomenon [12].

1.3.4 Molecule-electrode coupling

When molecule is coupled with an electrode, the discrete molecular energy levels mix with the continuum energy bands of the electrode and thus leading to changes in some of the properties of the molecule. In the simplest approximation of wide-band approximation, this only leads to a broadening of the energy level of the molecules. The lifetime of an electron then is inversely proportional to this broadening and hence determines the rate at which the electron can escape into the reservoir. In general the mixing of energy levels will lead to shift and broadening of the molecular energy levels. This is the case when other forms of self-energies like the Newns semi-elliptical form [46]is used instead of wide-band approximation. Hence a stronger coupling with electrode implies a higher current. Of particular importance is coupling of molecule to two different electrode, since the uneven coupling on both electrode with unequal voltage drop across the electrodes is predicted as means for obtaining negative differential resistance in molecular conductors.

1.3.5 Relative position of Fermi surface

In a typical scenario, the electrodes and the molecules are so selected that the Fermi level of the electrode (which is around -5 eV for noble metals) falls between the HOMO-LUMO of the molecules (approx -9 eV for HOMO). But once the connection is made, due to charge flow, charge rearrangement and geometric rearrangement, the Fermi level falls between the HOMO-LUMO gap. The charge flow and the allied process will continue to happen until the Fermi level falls within the gap. The Fermi level need not be halfway in between the HOMO-LUMO gap but could be anywhere in between. The above presented picture is somewhat simplified, in that, it presumes that the mixing between molecule and electrode is somewhat comparitively weaker than the interactions between the molecules. This may be true for most molecular-metal junctions but in case of molecular-semiconductor junctions needs serious rethinking, for these junctions are formed by strong covalent bonds.

1.3.6 Electrostatic potential profile inside the molecule

It is well known that the application of electric field shifts the electrochemical potential of the reservoirs. For electron transport through conductors , since field inside a conductor is zero, the voltage drops are assumed to occur at the junction and the voltage to remain a constant along the length of the conductor, while for semiconductors the voltage is expected to drop along the length of the semiconductor. The situation is somewhat in between for molecular transport. The potential profile inside the molecule depends on the strength of the coupling between the molecule-metal at the junction. A strong coupling will result in a ramp kind of potential profile while a weak coupling would result in majority of the voltage drop across the junction with a possible constant shift in the middle. The secondary factors which affect the potential profile inside the molecule are polarizability of the molecule and the charge distribution inside the molecule. In theory, the electrostatic potential in the absence of charge transport must satisfy poisson equation. In the presence of molecules, the potential needs to be determined consistently from the poisson equation with replacing the square of the wavefunction (the solution from

schrodinger eqaution) instead of the charge density. Density functional-NEGF calculation are employed in literature to carry out the above procedure [47, 48, 49, 50, 9, 51, 52].

1.3.7 Electronic structure of the molecule

Although conductance in dominated by electrons near the Fermi surface, in molecular transport, the bottle-neck of the phenomenon appears to be the availability of the number of channels for electron transfer. Irrespective of the materials involved, generally three different regions based on the channels available. The single transmission channel region occurs when the s band electrons dominate the DOS of the molecules. Similarly there exist 3 and 5 channels corresponding to p and d band electrons contributing the DOS [53] . The situation is further complicated due to hybridization. It is seen that not all available channels are used in conducting channels. Generally the dominant channel is a symmetric combination of orbitals in a hybridized view. This point of view is supported by certain experimental facts [54, 55, 56, 57, 58].

1.4 Mechanisms of electron transport

Broadly the electron transport is divided into three regimes: ballistic, diffusive and classical.

1.4.1 Ballistic regime

This type of transport regime is characterised with the sample size (l) much smaller than the momentum relaxation or phase relaxation length (l « L_m , « L_ϕ). This is ballistic since the electron can transport without loosing momentum and phase. The Landauer formalism holds good in this regime. The conductance is independent of the length of the

molecular wire. The conductance is due to the resistance at the contacts. In other words, it is scattering of electron at the boundary of reservoirs that determines the current. And hence the conductance is proportional to the width of the junction and independent of the length of the wire.

1.4.2 Diffusive regime

This regime is intermediate where $L_\phi >> L_m$ and the transport is diffusive. Since the electron retains it's initial phase , quantum interference effects still needs to be considered. The McConell [59] expression for rate of electron transfer holds valid in this regime. That is, G= A $exp(-\beta l)$ where, l is the length of the molecular wire, β is the characteristic decay parameter and A is some constant depending on the junction properties. In practice it has been found to be a good approximation for certain kind of alkanes up to a certain length and small voltages. One of the possible reasons for such behaviour is attributed to large HOMO-LUMO gap and the electron transfer takes place through super-exchange , a process where the electron hops through virtual orbitals which are energetically well separated from the electrode Fermi level.

1.4.3 Classical regime

This regime of transport happens when the size of the sample is larger than the momentum relaxation length and phase relaxation length. Interference effects can be neglected since the electron entering at one end looses information of it's initial phase. Inelastic scattering dominates in this regime and the conduction is that of a regular macroscopic wire obeying Ohm's law. In addition to inelastic and incoherent scatters, the electronic levels in the molecular wire couple to the vibration or other degrees of freedom present in the system resulting in a conduction dependent on the length of the sample.

1.5 Brief overview of theoretical tools

1.5.1 Lippman-Schwinger equation

This method was pursued primarily by Lang and co-workers [60, 61, 62, 63, 64] . The general mode of solving the problem is as follows: The bare metallic electrodes were considered in the presence of bias voltage and their single-particle wave-functions and density distributions were found using density-functional formalism. Next the bridge between the two electrodes are introduced and a Lippman-Schwinger equation is solved for each of the single-particle wavefunctions to obtain the wavefunction for the total electrodes plus bridge system. The density distribution is obtained from the wavefunctions and the solution is found by iterative procedure.

$$\psi(r) = \psi_0(r) + \int dr^{'} dr^{''} \mathrm{G}_0(r, r^{'}) \delta V(r^{'}, r^{''}) \psi(r^{''}) \tag{1.4}$$

In the above equation G_0 is the Green's function for the bare electrodes without the bridge and ψ_0 the wavefunction which describes the motion of electron in the two electrodes and δV is the difference in potential between the bare unconnected system and the one with bridged electrodes. The current is calculated by differentiating the expression for wavefunction obtained from solving the Lippman-Schwinger equation. Initially, Lang and co-workers approximated the wavefunction in the bare electrodes as plane waves [60, 65]. These were further refined by Joachin and Magoga [66, 67] who considered atomic orbitals instead of plane waves. In addition Joachim and co-workers employed recursive green's function methods and were able to obtain the exponential decay with increase in length of conductance.

1.5.2 Landauer-Buttiker Formalism

Landauer viewed current flow as a transmission process with electron entering the wire through on of the junctions and then calculating the probability for it to reach the other junction. Landauer employed the wave scattering to arrive at his result.

$$I = \frac{2e^2}{h} \int d\epsilon T(\epsilon)[f_L(\epsilon) - f_R(\epsilon)] \tag{1.5}$$

Where $T(\epsilon)$ is the transmission coefficient and f_L and f_R are the Fermi distributions function for the two electrodes. The prefactor $2e^2/h$ is known as the universal conductance and hence the numerical value of resistance is 12.9K Ω. The formula works well in case where the central region is small in comparison with the coherent length of the waves so that it is treated as purely elastic scattering without energy loss. Hence this formula is ideally suitable for ballistic thermal transport. The resistance is independent of the length of the conductor, the origin of which is at the junctions. Blencowe [68] made an estimation of the transmission coefficient using elastic wave models. Mode matching method [69, 70] is one of the prominently used technique for calculating Transmission coefficient. Wang and Co-Workers [71] calculated the transmission coefficient using scattering boundary method. Transfer matrix method have also been used to calculate the transmission coefficients in one dimensional atomic models as well as in continuum models.[72, 73, 74]

1.5.3 Ratner-Mujica Formulations

In 1994, Mujica, Ratner and Kemp [75, 76] developed a formalism to express current through a system of two electrodes connected by Molecular chains of N-sites. Initially, Mujica and Ratner considered explicitly the situation where the molecules in connected to the reservoirs only through the first and the last sites (1 and N). If Δ_L and Δ_R are the imaginary part of the self-energies contributions arising from the Left and Right reservoirs, then the expression for current as derived by Mujica and Ratner is

$$I(V) = \frac{4e}{\pi\hbar} \int_{E_F - eV/2}^{E_F + eV/2} \Delta_L \Delta_R |\mathrm{G}_{1N}|^2 dE \tag{1.6}$$

Some of the implicit assumption in the formalism is the absence of direct electrode-electrode interaction and imposing the condition that the reservoir and wire have orthogonal basis states. Mujica-Ratner employed atomic orbitals for basis functions. The

salient point to notice is that while the reservoir has basis function which are generally infinite dimensional, and the molecular wire has a finite dimensional basis function. But the relation expressing current depends only on the G of the molecule (that is, the Green's function of the molecule as modified by the possibly voltage dependent interaction with the reservoir and not the green's function of the free molecule), which is finite dimensional. It should also be noted that in the original work of Mujica-Ratner, the final current was not obtained by integrating over the energy levels between the two reservoirs modified appropriately by the voltage applies, but rather they assumed that current conduction is basically due to electrons near the Fermi surface and hence calculated the current profile by examining the form of the integrand near the Fermi surface. Yaliraki and Ratner [77] generalised the end-only connection assumption in the original work to arbitrary connections.

1.5.4 NEGF: Caroli's formula

A precise formula for calculating the current between two electrodes connected by a wire is given by Caroli and co-workers [78]. The original form of the derivation done was Caroli and co-workers by imposing certain additional constraints on the system and hence it was derived in a slightly restricted sense. The more widely accepted form for the formula is due to Wingreen and co-workers [79, 80, 81, 82]. They were able to obtain the formula while allowing certain additional interactions for the electrons in the wire. Both Caroli and Wingreen employed Kheldysh methods to obtain the formula. The same equation was also obtained by several other others by using Quantum Langevin Equations [83].

$$I(V) = \frac{e}{\pi\hbar}\int_{E_F-eV/2}^{E_F+eV/2} \mathrm{T}r[\mathrm{G}^r \Gamma_L \mathrm{G}^a \Gamma_R] dE \tag{1.7}$$

where $\mathrm{G}^{r\dagger} = \mathrm{G}^a$ is the green's function for the central wire region and $\Gamma_{L,R} = \Delta_{L,R}$ is the imaginary part of the self-energy arising out of the interaction between the wire and the electrodes. The problem, when expressed in the above formalism essentially boils down to evaluating elements of the green's function of the wire. This proceeds as follows

$$\begin{pmatrix} \epsilon \mathrm{I} - \mathrm{H}_L & -V_{LW} & 0 \\ -V_{WL} & \epsilon \mathrm{I} - \mathrm{H}_W & -V_{WR} \\ 0 & -V_{RW} & \epsilon \mathrm{I} - \mathrm{H}_R \end{pmatrix} \times \begin{pmatrix} \mathrm{G}_L & \mathrm{G}_{LW} & \mathrm{G}_{LR} \\ \mathrm{G}_{WL} & \mathrm{G}_W & \mathrm{G}_{WR} \\ \mathrm{G}_{RL} & \mathrm{G}_{RW} & \mathrm{G}_R \end{pmatrix} = \begin{pmatrix} \mathrm{I} & 0 & 0 \\ 0 & \mathrm{I} & 0 \\ 0 & 0 & \mathrm{I} \end{pmatrix} \tag{1.8}$$

Where $\mathrm{H}_{L,W,R}$ refers to the hamiltonian of the left, wire and the right reservoir, $V_{LW,RW,WL,WR}$ are the hopping terms from reservoir to wire. The quantity of interest is the green's function of the wire G_W. It should be noted that in general the $\mathrm{H}_{L,R}$ are infinite dimensional matrices and H_W is finite dimensional matrix. If the wire is modeled as N Single sites, then H_W is a matrix of N times N dimension. Solving for the green's function of the wire

$$\mathrm{G}_W = \frac{1}{\epsilon \mathrm{I} - \mathrm{H}_W - \Sigma_L - \Sigma_R} \tag{1.9}$$

In the above expression for G_W, the self energies $\Sigma_{L,R}$ arising from the electrode interaction are related to the $\Gamma_{L,R}$ in the Caroli's formulas as $\mathrm{I}m\Sigma_{L,R}$, and the $\Sigma_{L,R}$ can be expressed interms of the green's function of the electrodes $\Sigma_{(L,R)} = V^{\dagger}_{W(L,R)} G_L V_{(L,R)W}$. Thus even though the green's function of the molecular wire require an inversion of finite size matrix, the self-energies involve green's function of the electrode whose Hamiltonian's are infinite dimensional matrix. But this doesn't pose much of a problem as analytical solution are available for the form of green's function of the electrode.

1.5.5 Handling Interactions

The above mentioned theoretical methods generally do not address the question about the nature of specific interactions and their effect on the current. Of particular interest is the interaction of electron-phonons since these type of interactions are responsible for junction heating. It is well know that molecules are highly sensitive to temperature changes this issue needs to be addressed. It has been well-known from electrochemical literature [84, 85, 86, 87, 88, 89] that the transfer of electron from redox couple to electrodes has a different behaviour from transfer of electron from a single state to a con-

tinuum energy band. One possible mechanism is a one-step coherent transport process in which an electron tunnels via the redox state of the molecule from one electrode to another quickly so that the molecule has no time to relax to the reduced state, that is the molecule stays in the initial oxidized or reduced state for the whole duration of the electron transport. When the Fermi level matches with that of the redox energy level a large resonant tunneling current will be observed. Another possible proposed mechanism is a two stage process in which the electron tunnels to the redox and then resides in the redox until the redox relaxes to reduces state. Neither of the proposed models agrees well with the experiment and the more realistic assumption seems to imply that the net transfer process is a combination of both [43] .

1.6 Electron transfer and it's relevance in electrochemical environment

In electrochemistry, Self-Assembled Monolayers (SAM) play a vital role. Suitably designed SAMs can form organized assemblies with nano-particle arrays, metal-molecule contacts and structures resembling molecular wires. Two dimensional SAMs assembled on suitable sustrates are desired candidates for energy storage devices like fuel cells and in the fabrication of sensors and optoelectronic devices. A thorough knowledge of electron transfer mechanism in such orgnaized assemblies is neccessary for the successfull applications. A theoretical approach in addressing the problem of electron transfer in SAMs will help greatly in identifing ideal molecular assemblies.

1.6.1 Bridge mediated electron transfer

The bridge mediated electron transfer process is known to be a prominent electron transfer mechanism in many biological structures like redox proteins, photosynthetic reaction, nucleic acids etc [59, 90, 91, 92, 93, 94, 95] . The electronic coupling through

a chain linking an electron donor to an acceptor can control the rate of electron transfer between the groups on the two chain ends. Electrochemical techniques are well suited for the studies of long range electronic coupling and electron transfer between metal electrodes and attached redox molecules [96]. Electron transfer can be investigated with the help of techniques like voltammetry and impedance measurements. Two dimensional SAMs can be designed to study the distance dependency in long range bridge mediated electron transfer [97, 98, 99, 100].

It has been well known from the works of A. J. Bard and co-workers [96, 101], that organized monolayers of alkane thiols on electrodes provide a general route to creating surface structures in which redox species are linked to electrodes through molecular bridges whose length and structure can be varied. Furthermore, Dubois and Nuzzo [102] designed SAMs of alkane thiol molecules on a gold surface which provided a convienent approach for studying electron transfer reaction between and electroactive group and electrode where the electroactive group is held at fixed distance from the electrode surface. Typically, distance dependencies of electron transfer is mainly investigated with redox molecules like ferrocene and ferrocyanide ions. For example, hexacyanoferrate species in assemblies is a well studied one due to it's potential application in catalysis and sensors. It is possible to study electron transfer rate in biological species using methods developed in electrochemistry. For example, cytochrome C is a biomolecule. It's electroactivity is due to it's porphyrin skeleton. By linking porphyrin / cytochrome as the terminal group of alkane thiols of different chain length, the distance dependency of electron transfer has been investigated [103, 104].

1.6.2 Electrochemical coulomb staircase charging

Monolayer Protected Cluster (MPC) has demonstrated an electrochemical analogue of coulomb staircase charging. Clusters of Au, Ag, Pt etc. are stabilised by protection by ligand monolayers of alkanethiols, silanes, polymers etc. Due to the combination of small metal - like core size and hydrocarbon like dielectric coating, the capacitance of

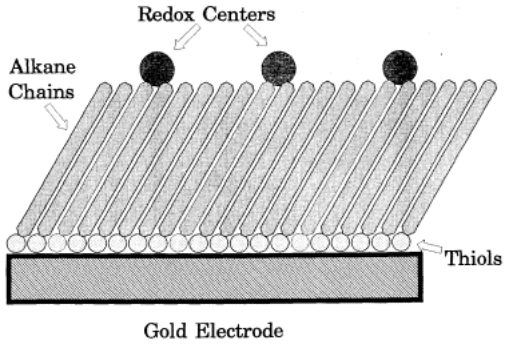

Figure 1.1: An ideal Self Assembled monolayer based on alkanethiols assembled on gold electrode. (source: page 240, in Electroanalytical chemicstry: a series of advances, vol 19. by A. J. Bard and I. Rubinstein)

the MPC is less than an attofarad per MPC. Thus addition or removal of singel electron from such capacitors produces potential changes so that the solution phase, double layer capacitance charging of MPCs becomes a quantized [105, 106]. A theoretical modelling of the above mentioned scenario starts with a simple electrostatic interaction. Theories have been further extended to account for the microelectrode character of the clusters [107, 108].

1.6.3 Electrocatalysis

Three dimensional SAMs are expected to be of significant importance in the catalysis of fuel cells. Preparation of catalyst in the form of nano-particles assemblies increases the surface area to a large extent and hence the efficiency of catalysis also increases. This helps in the fabrication of miniaturized fuel cells. Since oxidation of organic fuels is the primary process in fuel cells, a thorough understanding of electron transfer in such scenarios help in developing fuel cells with a overall higher performance.

1.7 Organization of Thesis

The thesis is organized as follows.

Chapter 2: We present the calculation and results for conductivity of a molecular wire containing a redox center, and embedded in an electrochemical environment. The effect of solvent modes interactions with the redox were included and an exact expression for quantum conductance for a chain of arbitrary length is derived. Thermal averages were handled numerically and explicit plots for I-V profile are provided for three atoms case. Plots showing rectification, extended current voltage plateaus, negative differential resistances are included.

Chapter 3: We discuss the rate of electron transfer from a redox to an electrode via N-atom bridge. The redox interacts in an electrochemical environment with solvent modes. A model hamiltonian for such a system is presented employing which a voltage dependent expression for rate is provided. The variation of electron transfer rate with various parameters like coupling strength, re-organisation energies etc. are analysed numerically. In particular, graphs showing a complete blocking of electron transfer in suitable voltage range for certain coupling strengths are presented.

Chapter 4: We explain in detail the role of adsorbate coverage on the electron transfer between a solvated redox and adsorbate-electrode complex. The inherent randomness involved in the distribution of adsorbates in the substrate surface is handled using Coherent Potential Approximation (CPA). Current-Overpotential plots are provided for all regimes of coverage factor and strong and weakly couplied adsorbate-substrate interactions are analysed specifically. It is shown that in the low coverage regime, adsorbate mediated electron transfer exhibits the characteristics of homogeneous electron transfer while in high coverage regime the direct heterogeneous electron transfer behaviour is obtained.

Conclusion: We conclude with an overview of the work, and future directions of research based on this work.

Chapter 2

Electron tunneling between two electrodes mediated by a molecular wire containing a redox center

2.1 Introduction

Understanding of electron transport through a single molecules received an increased interest due to the speculation of employing molecular units as fundamental elements of computer circuits [5, 6]. Additionally, electron transfer in molecular wires at nanoscale level received further attention, both at the level of formalism as well as ab-initio calculations, due to its possible relevence in understanding and application for a class of diverse problems like sensors, photonics, solar energy conversion [109]. Controlled charge movement in a suitably designed molecule can be used as the basis for storing and processing of information. Such Quantum-Dot Cellular Automata architecture has been experimentally realised in a series of experiments for a variety of applicable components like memory cells, logic gates and clocked memory cells[110, 111, 112]. A practical implementation of QCA architecture consists of a single redox center with an organic or inorganic bridging group [113]. The efficiency of solar energy conversion process depends not only on efficient photon capture but also on charge seperation and transport through very large distances. Since the charges are created by sunlight on the surface of an assembly of molecules or semiconductors, it is resonable to expect molecular wires to act as

relevant acceptors of the charges. Also the weak solar fluxes imply a very low current and a need for fast charge transport. Certain classes of polymers and oligomers have been proposed as ideal candidates for satisfying the above criterion for increasing the yield in solar energy conversion [114, 115].

The above mentioned are some of the reasons for the recent increased surge in interest for understanding charge transport along molecular wires. Typical theoretical work in the field involves obtaining generic expressions for the conductance, current-voltage profiles, rate constants, transition probabilites etc. Formal works on transport properties along molecular wires were carried out on Donor-Bridge-Acceptor (DBA complexes) systems, wherein electrons are transferred between donor and acceptor connected by a molecular bridge [116, 117, 16, 59]. Further, electron transfer between reservoirs connected by a molecular bridge has been studied by Ratner and co-workers [75, 76, 118]. The above works resort to time-dependent quantum mechanics for obtaining expressions relevant to electron transfer. Expressions for the conductance between two reservoirs connected by monoatomic sites were well known in mesoscopic physics. The formal expression was first derived by Caroli and co-workers [78] and was later expanded to a broader class of problems by Wingreen and co-workers [79, 80, 81]. Recently, the same expressions were re-derived by various authors [119, 120, 121, 122, 83] by formulating Quantum Langevin Equations (QLE). Initially, both the molecular wire and mesoscopic conduction were modelled using tight-binding Hamiltonians, and since at a Hamiltonian level these problems seem identical, it is expected that the expression obtained for one should be applicable for the other.

Several authors have pursued other computational methods such as density functional theory, first principle ab-initio calculations and package simulation of Non-Equilibrium Green's Function in studying conduction through molecular wires [52, 123, 124, 125, 126]. Most of these authors differ in their treatment of the electrodes and the interaction of the metal-molecule coupling. Most of the earlier works were oriented towards a better approximation for modelling the interaction and self-energies at the molecule-metal junctions, while little work has been done in incorporating the effect of additional interactions the electron might experience in the molecular wires. Though numerous works have been done of the subject of electron-phonon coupling with relevance to quantum dots [79, 127, 128, 129, 130, 131, 132], including treatments for classical, quantum, equi-

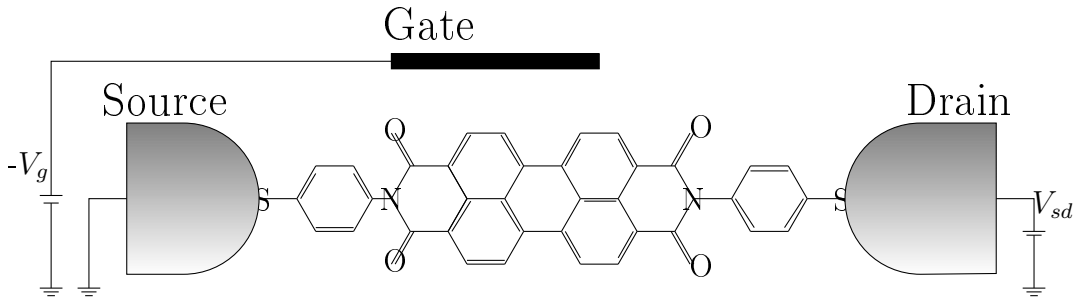

Figure 2.1: Schematic of a gated molecular transistor in an electrochemical environment (see ref.[1])

libriated and out of equilibrium systems, exact treatment of such a process in specific for molecular wire has not received much attention. Molecular wires differ from quantum dots in that the observed conductance behaviour of quantum dot is dominated by Coloumb blockade.

The focus in the present will be on a special electrochemical case: a molecular wire containing a redox-center connecting two electrodes. The electrochemical case is of special interest since two potentials can be varied independently: the bias between the two electrodes, and the potential of one of the electrodes with respect to the solution. The latter acts like a gate voltage that controls the current in the wire. In addition, the redox center interacts with the solvent, whose fluctuation will affect the current. The specialties of the electrochemical situation were first elucidated by theorists [133, 134, 135, 136]. Starting with the pioneering paper of Tao [1], there have been a fair number of experimental studies of electrochemical systems [137, 138, 139, 43, 36, 140, 141, 142, 143, 144] which in turn have generated more theoretical work (see e.g. [145, 146] and references therein).

Most of the theoretical work on electrochemical systems has been restricted to special systems with one or two intervening redox centers. In this study, we will consider a wire of arbitrary lengths containing one redox center interacting with the solvent. Using a tight-binding Hamiltonian and Green's function techniques we will derive an expression

for the current which is exact for the case where the interaction to the two electrodes can be treated in the wide-band approximation. These calculations will be illustrated by model calculations for particularly interesting cases: steps and negative differential resistance, and spectroscopy of intermediate electronic states.

2.2 Model Hamiltonian, Green's functions and current density

The model system that we consider consists of two metal electrodes, labeled R and L, connected by a chain of $2n+1$ atoms – an odd number is chosen for convenience only. The atom in the center is redox-active and interacts with the solvent; thus, we identify the index $n+1$ with the index r of the redox species. We use a tight-binding model, in which each atom contains one orbital and interacts only with its nearest neighbor. The corresponding Hamiltonian can be written in the form:

$$\begin{aligned}\mathbf{H} = &\sum_k \sum_{i=L,R} \epsilon_{k,i} n_{k,i} + \epsilon_r n_r + \sum_{\substack{i=1 \\ i\neq n+1}}^{2n+1} \epsilon_i n_i \\ &+ \sum_{i=1}^{n-1} \{v_i c_i^\dagger c_{i+1} + h.c\} + \sum_{i=n+2}^{2n} \{v_i c_i^\dagger c_{i+1} + h.c\} \\ &+ \sum_{i=n,n+1(r)} \{\bar{v}_i c_i^\dagger c_{i+1} + h.c\} + \sum_k \{v_{k,1} c_{k,L}^\dagger c_1 + v_{k,2n+1} c_{k,R}^\dagger c_{2n+1} + h.c\} \\ &+ \frac{1}{2} \sum_\nu \hbar\omega_\nu q_\nu^2 + \sum_\nu \hbar\omega_\nu g_\nu q_\nu n_r \end{aligned} \tag{2.1}$$

In this Hamiltonian, n always denotes an occupation number, $c^\dagger$ a creation c an annihilation operator, ϵ an energy, and v a coupling constant. The first line contains the diagonal elements, the indices (k, L) and (k, R) labeling the electronic states on the two electrodes. The second and third lines give hopping elements between adjacent sites, and the last line the potential energy of the solvent, with coordinates q_ν and frequencies ω_ν, and its interaction with the redox center r; the g_ν are the corresponding coupling constants. Equation (2.1) is a natural generalization of the Hamiltonian for redox-mediated tunneling via one center [136].

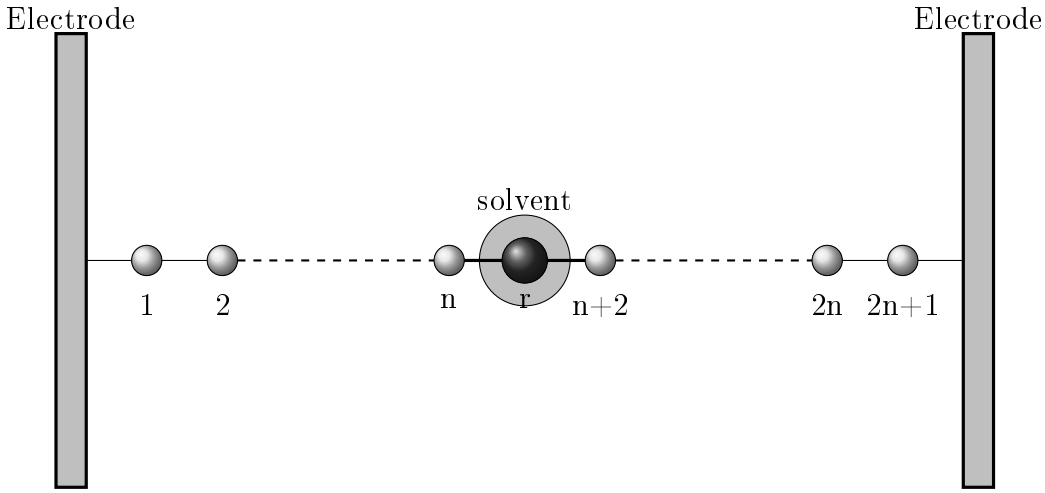

Figure 2.2: Simple schematic of a molecular wire stretched between two electrode with an redox center interacting with the polarization of the surrounding solvent.

The matrix form of the fermionic part of the above Hamiltonian H_F has the generic form:

$$\mathbf{H_F} = \begin{pmatrix} \epsilon_{k,L} & v_k & 0 \\ v_k & \mathbf{H}_{chain} & v_k \\ 0 & v_k & \epsilon_{k,R} \end{pmatrix}$$

$$\mathbf{H}_{chain} = \begin{pmatrix} \epsilon_1 & \upsilon & & & & & \\ \upsilon & \epsilon_2 & \ddots & & & & \\ & \ddots & & \bar{\upsilon} & & & \\ & & \bar{\upsilon} & \epsilon_r + \lambda_\nu q_\nu & \bar{\upsilon} & & \\ & & & \bar{\upsilon} & & \ddots & \\ & & & & \ddots & & \upsilon \\ & & & & & \upsilon & \epsilon_{2n+1} \end{pmatrix}_{2n+1 \times 2n+1}$$

Working within the nearest neighbour interacting tight-binding model, it is understood that $\mathbf{H}_F$ has non-zero entries only in diagonal and sub-diagonal elements. The general scheme of approach is to calculate the quantum conductance and then obtain the current by integrating the conductance between appropriate limits. The formula employed for obtaining the quantum conductance, or tunneling rate, is the same as the one

used by Datta *et al.* [147]. This form of the formula was first derived by Caroli *et al.* [78] and was subsequently derived in a much wider context by Wingreen and co-workers [79, 80, 81].

$$g = \mathrm{T}r[\mathrm{G}^r \Gamma_L \mathrm{G}^a \Gamma_R] \tag{2.2}$$

As before, the subscripts L and R refer to the left and right reservoir. Γ denotes the imaginary part of self-energy (for ease of following the notations, $\Gamma = v_k(ImG^0_{kk})v^*_k$). The quantity of interest is $\mid \langle 1 \mid G \mid 2n+1 \rangle \mid^2$, where G is the Green's function obtained from the above Hamiltonian. This can be obtained by separating the Hamiltonian into two parts: $\mathbf{H} = \mathbf{H}_0 + V$ and considering a Dyson equation , $G = G^0 + G^0 V G$, where the simplification of the problem results from the choice of V. Letting $V = \sum_{i=n,n+1} \bar{v}_i c^\dagger_i c_{i+1} + h.c$, the Hamiltonian $\mathbf{H}^0_F$ contains 3 block matrices. Physically this amounts to cutting the $2n+1$ atom chain at 2 places on either side of the redox couple. The closed form for the element $\langle 1 \mid G \mid 2n+1 \rangle$ is obtained as shown:

$$\begin{aligned} \langle 1 \mid G \mid 2n+1 \rangle &= \langle 1 \mid G^0 \mid 2n+1 \rangle + \sum_{i,j} \langle 1 \mid G^0 \mid i \rangle \langle i \mid V \mid j \rangle \langle j \mid G \mid 2n+1 \rangle \\ &= \langle 1 \mid G^0 \mid n \rangle \langle n \mid V \mid n+1 \rangle \langle n+1 \mid G \mid 2n+1 \rangle \end{aligned} \tag{2.3}$$

$$\begin{aligned} \langle n+1 \mid G \mid 2n+1 \rangle &= \langle n+1 \mid G^0 \mid n+1 \rangle \langle n+1 \mid V \mid n \rangle \langle n \mid G \mid 2n+1 \rangle \\ &+ \langle n+1 \mid G^0 \mid n+1 \rangle \langle n+1 \mid V \mid n+2 \rangle \langle n+2 \mid G \mid 2n+1 \rangle \end{aligned} \tag{2.4}$$

$$\langle n \mid G \mid 2n+1 \rangle = \langle n \mid G^0 \mid n \rangle \langle n \mid V \mid n+1 \rangle \langle n+1 \mid G \mid 2n+1 \rangle \tag{2.5}$$

$$\begin{aligned} \langle n+2 \mid G \mid 2n+1 \rangle &= \langle n+2 \mid G^0 \mid 2n+1 \rangle \\ &+ \langle n+2 \mid G^0 \mid n+2 \rangle \langle n+2 \mid V \mid n+1 \rangle \langle n+1 \mid G \mid 2n+1 \rangle \end{aligned} \tag{2.6}$$

From the above 4 equations , $G_{1,2n+1} = \langle 1 \mid G \mid 2n+1 \rangle$ can be solved:

$$G_{1,2n+1} = \frac{G^0_{1,n}\bar{\upsilon}_{n,n+1}G^0_{n+1,n+1}\bar{\upsilon}_{n+1,n+2}G^0_{n+2,2n+1}}{1 - G^0_{n+1,n+1}[\bar{\upsilon}_{n+1,n}G^0_{n.n}\bar{\upsilon}_{n,n+1} + \bar{\upsilon}_{n+1,n+2}G^0_{n+2,n+2}\bar{\upsilon}_{n+2,n+1}]} \tag{2.7}$$

Now we require the terms $G^0_{1.n}, G^0_{n+1,n+1}, G^0_{n+1,n+2}, G^0_{n+2,2n+1}, G^0_{n+2,n+2}$. These can be found by using the above reduced Green's function technique, in addition to exploiting the recursive relation for the determinant of a matrix consisting only of diagonal and subdiagonal entries. Similar calculational methods were employed by Evenson and Karplus [148].

For simplicity, we assume that the couplings to the two metals at the ends are the same, and use the wide-band approximation, in which $\Delta = \pi \sum_k \mid v_k \mid^2 \delta(\epsilon - \epsilon_k)$ is taken as constant.

If d_n represents the determinant of a $n \times n$ matrix with diagonal entries set to $\epsilon - \epsilon_i$ and subdiagonal entries set to some υ, then it is possible to express:

$$G^0_{1,n} = \frac{(-\upsilon)^{n-1}}{d_n - d_n[\frac{v_k^2}{\epsilon - \epsilon_k}]} \tag{2.8}$$

$$G^0_{n,n} = \frac{d_{n-1} - d_{n-2}[\frac{v_k^2}{\epsilon - \epsilon_k}]}{d_n - d_{n-1}[\frac{v_k^2}{\epsilon - \epsilon_k}]} \tag{2.9}$$

$$G^0_{n+1,n+1} = \frac{1}{\epsilon - \epsilon_r} \tag{2.10}$$

$$G^0_{n+2,2n+1} \cong G^0_{1,n} \tag{2.11}$$

$$G^0_{n+2,n+2} \cong G^0_{n,n} \tag{2.12}$$

Invoking the wide band approximation the above expressions reduce to the following form:

$$G^0_{1,n} = \frac{(-\upsilon)^{n-1}}{d_n + i d_n \Delta} \tag{2.13}$$

$$G^0_{n,n} = \frac{d_{n-1} + i d_{n-2}\Delta}{d_n + i d_{n-1}\Delta} \tag{2.14}$$

Thus, the problem has been reduced to calculating the determinants d_n, which will be thoroughly explained in the next chapter.

The conductance can be obtained from Caroli's formula and integrated to obtained the net current. The net current thus obtained has a q_ν dependency which has to be eliminated by performing a thermal averaging. The final result obtained after thermal averaging gives the net total current. As noted in the introduction, in electrochemical systems there are two potential differences to consider: the bias V between the two electrodes, and the electrode potential, which shifts the levels in the solution. We use the convention that the potential of the right electrode R is kept constant, and set its Fermi level to zero. The levels on the wire shift with the electrode potential; this assumes that the conductivity of the solution is higher than that of the wire. Other scenarios can be calculated by the same formalism. With this convention, we write the total current in the form:

$$I(q) = \int \mathrm{T}r[\mathrm{G}^r \Gamma_L \mathrm{G}^a \Gamma_R]\{f(\epsilon + e_0 V) - f(\epsilon)\} d\epsilon \tag{2.15}$$

where $f(\epsilon)$ denotes the Fermi-Dirac distribution. As has been pointed out several times (see e.g. [149]), in the case of a classical solvent it is sufficient to consider a single effective solvent coordinate q. Effectively, this means that in the Hamiltonian, we make the following substitutions:

$$\frac{1}{2}\sum_\nu \hbar\omega_\nu a_\nu^2 \;\rightarrow\; \lambda q^2, \qquad \sum_\nu \hbar\omega_\nu g_\nu q_\nu \;\rightarrow\; -2\lambda q \tag{2.16}$$

The average over the solvent configurations can then be written as:

$$I = \frac{1}{Z}\int dq e^{-\beta E(q)} I(q) \qquad Z = \int dq e^{-\beta E(q)} \tag{2.17}$$

where the energy, as a function of the solvent coordinate q, is:

$$E(q) = \lambda q^2 + \sum_i \int \epsilon \langle c_i^\dagger c_i \rangle \tag{2.18}$$

Thus $E(q)$ is obtained by performing a partial trace over the fermionic part of the total Hamiltonian. The quantity $\langle c_i^\dagger c_i \rangle$, as viewed by Wingreen et al. [79], is the lesser component of the Keldysh Green's function, $\mathrm{G}_{ii}^<$. If Γ_L and Γ_R are the imaginary parts of the self-energy arising from the interaction with the left and the right reservoirs (which in the view of wide-band approximations is Δ), then for the present case

$$\mathrm{G}_{ii}^< = if(\epsilon + e_0 V)[\mathrm{G}^r \Gamma_L \mathrm{G}^a]_{ii} + if(\epsilon)[\mathrm{G}^r \Gamma_R \mathrm{G}^a]_{ii} \tag{2.19}$$

At this point, a few comments on the appearance for $\mathrm{G}^<$ are needed. It is well known that in equilibrium the lesser Green's function takes the form of a product of spectral function times the occupation function. ($\mathrm{G}^< = ia(\epsilon)f(\epsilon)$). That is in case of zero bias V when both the reservoirs have the same potential, $f(\epsilon + e_0 V) = f(\epsilon)$, then

$$\mathrm{G}^< = if(\epsilon)[\mathrm{G}^r(\Gamma_L + \Gamma_R)\mathrm{G}^a] = if(\epsilon)2\Delta[\mathrm{G}^r \mathrm{G}^a] \tag{2.20}$$

Now $\mathrm{G}^r(\epsilon) - \mathrm{G}^a(\epsilon) = a(\epsilon)$ where $a(\epsilon)$ is the spectral function, and the imaginary part of self-energy can be written as $(1/\mathrm{G}^a - 1/\mathrm{G}^r)$. In our notation, $2\Delta = \Delta_L + \Delta_R = (1/\mathrm{G}^a - 1/\mathrm{G}^r)$. Also the diagonal part of $\mathrm{G}^r(\epsilon) - \mathrm{G}^a(\epsilon)$ is proportional to the density of states, $\rho(\epsilon)$. In equilibrium, we recover the result

$$\mathrm{G}^< = if(\epsilon)a(\epsilon) = f(\epsilon)(\mathrm{G}^r - \mathrm{G}^a). \tag{2.21}$$

Substituting the above result in the expression (2.18) for $E(q)$, it is seen that at equilibrium $E(q) = \lambda q^2 + \int \epsilon f(\epsilon) \mathrm{Im}\mathrm{Tr} G(\epsilon) d\epsilon$, wherein the second term in the energy expression is widely employed in a variety of contexts in physics. Thus the expression for $E(q)$ for the non-equilibrium case can be written compactly as

$$E(q) = \lambda q^2 + \int \epsilon f(\epsilon + e_0 V)\mathrm{Tr}[\mathrm{G}^r \Gamma_L \mathrm{G}^a] d\epsilon + \int \epsilon f(\epsilon)\mathrm{Tr}[\mathrm{G}^r \Gamma_R \mathrm{G}^a] d\epsilon \tag{2.22}$$

The trace in the above equation runs over the $(2n+1)$ sites numbered by the index i. Now for better exposition of the computation involved in calculating the $E(q)$, we consider a generic term which has the form shown below:

$$E_i(q) = \Delta \int_{-\infty}^{0} \epsilon \mathrm{G}_{i,1}^r \mathrm{G}_{1,i}^a d\epsilon + \Delta \int_{-\infty}^{-eV} \epsilon \mathrm{G}_{i,2n+1}^r \mathrm{G}_{2n+1,i}^a d\epsilon \tag{2.23}$$

where we have replaced the Fermi-Dirac distribution by step function, and taken the

Fermi level as zero.

We consider the case for the three possible locations of i, $(i \leq n, i \geq n+2, i = n+1)$. As before the general idea behind the approach to get the matrix elements of G is to resort to a Dyson expansion. The closed form equation so obtained has to be solved to get the relevant terms. The choice of V is same as used before.

$$\mathrm{G}_{1,i} = \mathrm{G}^0_{1,i} + \mathrm{G}^0_{1,n}\bar{v}_{n,n+1}\mathrm{G}_{n+1,i} \tag{2.24}$$

$$\mathrm{G}_{n+1,i} = \mathrm{G}^0_{n+1,i} + \mathrm{G}^0_{n+1,n+1}\bar{v}_{n+1,n+2}\mathrm{G}_{n+2,i} + \mathrm{G}^0_{n+1,n+1}\bar{v}_{n+1,n}\mathrm{G}_{n,i} \tag{2.25}$$

$$\mathrm{G}_{n+2,i} = \mathrm{G}^0_{n+2,i} + \mathrm{G}^0_{n+2,n+2}\bar{v}_{n+2,n+1}G_{n+1,i} \tag{2.26}$$

$$\mathrm{G}_{n,i} = \mathrm{G}^0_{n,i} + \mathrm{G}^0_{n,n}\bar{v}_{n,n+1}\mathrm{G}_{n+1,i} \tag{2.27}$$

Case I: $i \leq n$

$$\mathrm{G}_{1,i} = \mathrm{G}^0_{1,i} + \frac{\mathrm{G}^0_{1,n}\bar{v}_{n,n+1}\mathrm{G}^0_{n+1,n+1}\bar{v}_{n+1,n}\mathrm{G}^0_{n,i}}{1 - [\mathrm{G}^0_{n+1,n+1}\bar{v}_{n+1,n+2}\mathrm{G}^0_{n+2,n+2}\bar{v}_{n+2,n+1} + \mathrm{G}^0_{n+1,n+1}\bar{v}_{n+1,n}\mathrm{G}^0_{n,n}\bar{v}_{n,n+1}]} \tag{2.28}$$

$$\mathrm{G}^0_{1,i} = \frac{(-v)^{i-1}d_{n-i}}{d_n + i\Delta d_{n-1}} \tag{2.29}$$

$$\mathrm{G}^0_{n,i} = \frac{(-v)^{n-i}(d_{i-1} + id_{i-2}\Delta)}{d_n + i\Delta d_{n-1}} \tag{2.30}$$

Case II: $i \geq n+2$

$$\mathrm{G}_{1,i} = \frac{\mathrm{G}^0_{1,n}\bar{v}_{n,n+1}\mathrm{G}^0_{n+1,n+1}\bar{v}_{n+1,n+2}\mathrm{G}^0_{n+2,i}}{1 - [\mathrm{G}^0_{n+1,n+1}\bar{v}_{n+1,n+2}\mathrm{G}^0_{n+2,n+2}\bar{v}_{n+2,n+1} + \mathrm{G}^0_{n+1,n+1}\bar{v}_{n+1,n}\mathrm{G}^0_{n,n}\bar{v}_{n,n+1}]} \tag{2.31}$$

It is crucial to note at this stage that because of the form of perturbation selected the unperturbed G^0 has a symmetric structure with respect to the first and third block matrix and hence $\mathrm{G}^0_{n+2,i}$ in the above is same as $\mathrm{G}^0_{1,i}$ in case I.

Case III: $i = n+1$

$$\mathrm{G}_{1,n+1} = \frac{\mathrm{G}^0_{1,n}\bar{v}_{n,n+1}\mathrm{G}^0_{n+1,n+1}}{1 - [\mathrm{G}^0_{n+1,n+1}\bar{v}_{n+1,n+2}\mathrm{G}^0_{n+2,n+2}\bar{v}_{n+2,n+1} + \mathrm{G}^0_{n+1,n+1}\bar{v}_{n+1,n}\mathrm{G}^0_{n,n}\bar{v}_{n,n+1}]} \tag{2.32}$$

Even though $\bar{v}_{n,n+1} = \bar{v}_{n+1,n+2} = \bar{v}$, we have maintained the subscript indices for ease of checking the final expressions.

2.3 Results and discussions

The principle new feature of our work is the dynamic interaction of the redox system with the adjoining species, which fluctuates with the solvent coordinate q. The main effects can be demonstrated with a chain of three atoms, and we limit our numerical calculation to this case.

Even though we have restricted our treatment to the symmetric case, in which the coupling Δ to the two leads and the interatomic couplings v are the same on both sides, the system contains a fair amount of parameters. In the following model calculations, we have set $\Delta = 0.3$ eV and the reorganization energy $\lambda = 0.3$ eV unless otherwise mentioned, and for the other parameters we have chosen values appropriate to demonstrate special effects.

The case of a single intervening redox center is well examined. The new feature of the three-atom chain is the interaction between the levels ϵ_1 of the two side atoms and the redox center. Before considering this in detail, it is instructive to investigate the reference case in which this effect is weak; in this limit, we should obtain similar results to the case of one atom.

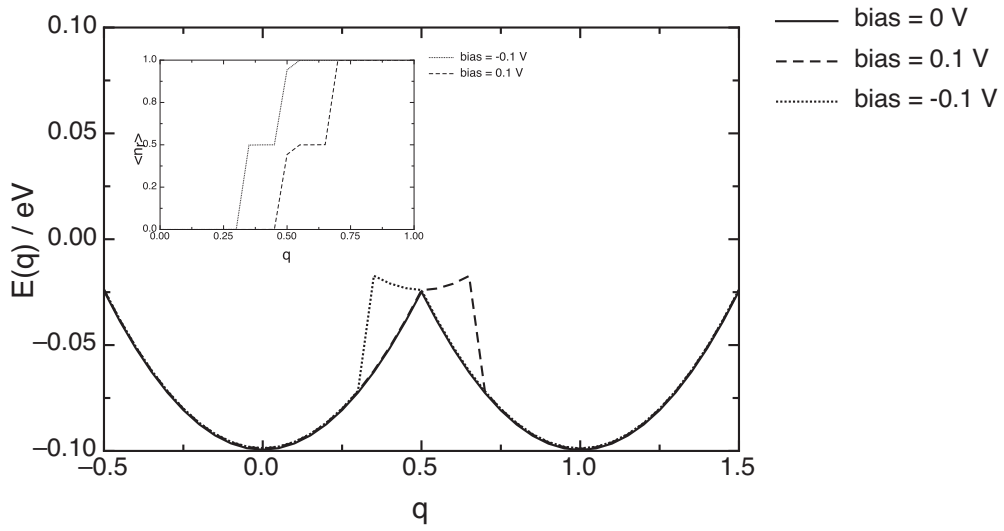

Figure 2.3: Potential energy surfaces in the case of weak coupling and at the equilibrium potential for the redox system; system parameters: $\epsilon_1 = 0.8$ eV, $v = 0.01$ eV, $\epsilon_r = \lambda = 0.3$ eV. The insert shows the occupation $\langle n_r \rangle$ of the redox center.

The interaction of the side atoms with the center is weak, if ϵ_1 lies far from the Fermi level and the coupling v is small. In this limit, the redox center is at the equilibrium

potential for $\epsilon_r = \lambda$. As expected, in this case the potential energy surfaces $E(q)$ are similar to the one atom case [150]. At zero bias, they have the same form as for a normal, outer sphere redox reaction- see Fig. 2.3. In the left well, the occupancy $\langle n_r \rangle$ is zero, in the right well unity. Application of a bias produces a region with $\langle n_r \rangle \approx 1/2$, which extends the barrier in the center. For the three atom case, the tunneling rate, as a function of the electronic energy ϵ and the solvent coordinate q, is given by:

$$t(\epsilon, q) = \frac{\Delta^2 \bar{v}^4}{(\epsilon - \epsilon_r + 2\lambda q)^2 \left[(\epsilon - \epsilon_r + 2\lambda q)(\epsilon - \epsilon_1 + i\Delta) - 2\bar{v}^2\right]^2} \tag{2.33}$$

As long as ϵ_1 lies so high that it plays no role, this rate has a maximum where $\epsilon - \epsilon_r + 2\lambda q = 0$. Tunneling occurs only between the two Fermi levels, in the range $-e_0 V < \epsilon < 0$. Inspection shows, that the maximum of $t(\epsilon, q)$ is obtained in the region where $\langle n_r \rangle \approx 1/2$, which therefore gives the main contribution to the current.

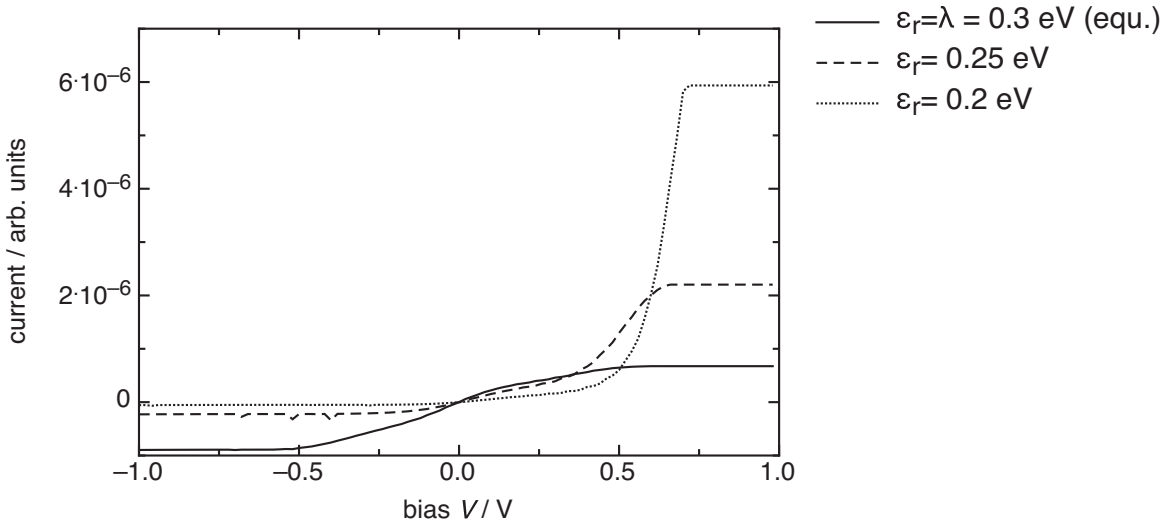

Figure 2.4: Current-potential curves in the case of weak coupling; system parameters: $\epsilon_1 = 1.2$ eV, $v = 0.01$ eV.

Continuing with the case of weak coupling, the current-potential curves are symmetric at the equilibrium condition $\epsilon_r = \lambda$. Shifting ϵ_r by application of an overpotential leads to asymmetrical curves with rectifying properties. Figure 2.4 shows the case in which the redox level has been lowered, so that the most favorable energy range now lies below the Fermi level of the right electrode. Therefore the current is higher at positive bias, where this energy range lies between the two Fermi levels.

Really new features occur when the redox level interacts noticeably with the levels ϵ_1. In general, three interacting atomic levels combine to form three molecular orbitals. Since the redox level changes its energy with the solvent fluctuations, so do the resulting molecular orbitals. So, for some range of q the redox level will be far from ϵ_1 and the interaction will be almost negligible, in another range it will lie close in energy, so that one observes the typical splitting of the levels.

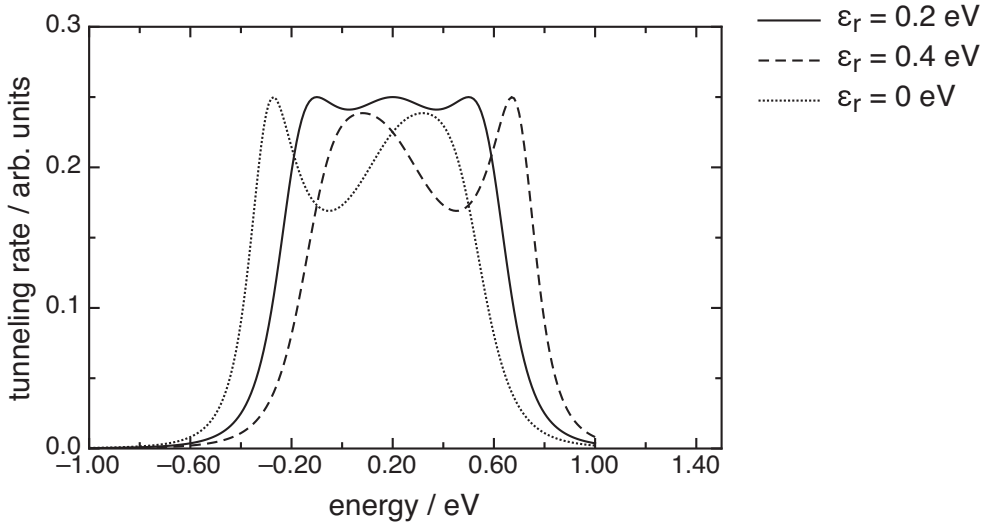

Figure 2.5: Transition probability as a function of the energy ϵ of the tunneling electron for various values of ϵ_r; the solvent coordinate q was set to zero. System parameters: : $\epsilon_1 = 0.2$ eV, $v = 0.1$ eV.

The transition probability $t(\epsilon, q)$ has local maxima, whenever ϵ is near one of the molecular orbitals. Since is depends only on the combination $\epsilon_r - 2\lambda q$, it is sufficient to investigate the dependence on ϵ_r for $q = 0$, as is done in Fig. 2.5. The interesting region lies where $\epsilon_r \approx \epsilon_i$. When both are equal, there are three distinct maxima at the three molecular orbitals. When they are separated, only two maxima occur at the position of the atomic orbitals, since the splitting is too small to show up – it is hidden beneath the maxima.

These oscillations in the transition probability give rise to interesting current-potential curves exhibiting several steps and even regions with a negative differential resistance (see Fig. 2.6), effects which do not occur with a single electronic intermediate state. The exact shape of these characteristics is determined by an interplay of three effects: The change of the potential-energy curves with the bias, the dynamic changes in the energy of the molecular orbitals as the solvent coordinate q fluctuates, and the resulting

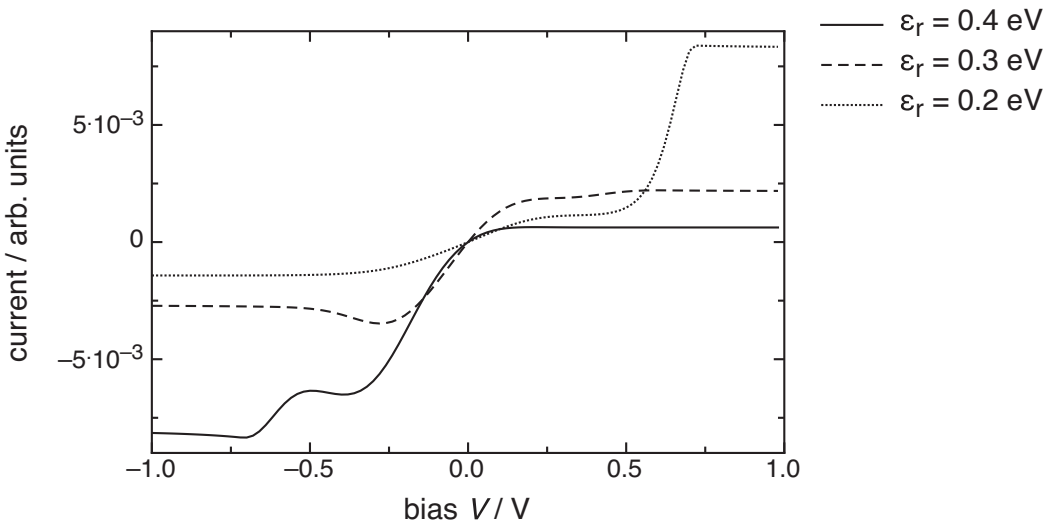

Figure 2.6: Current-potential curves for various values of ϵ_r. System parameters: : $\epsilon_1 = 0.2$ eV, $v = 0.1$ eV.

oscillations in the transition rate. These highly nonlinear effects are more pronounced when the coupling Δ to the two leads is weaker. Figure 2.7 shows two examples where the system parameters have been chosen such that the curves either exhibit nice plateaus or a pronounced negative differential resistance.

As pointed out in the introduction, in electrochemical systems two voltages can be controlled independently, the bias and the potential between the solution and one electrode. This makes it possible to perform spectroscopy of the electronic states in the wire, which experience the potential of the solution. We introduce the overpotential η of the redox couple with respect to the right electrode through $\epsilon_r = \lambda - e_0\eta$, and let the intermediate state shift in the same way: $\epsilon_1 = \epsilon_1^0 - e_0\eta$. In a real system, because of the finite conductivity of the solution, η may be only a fraction of the externally applied potential, but this would require only a trivial modification. If we keep the bias constant at a comparatively small value and scan the overpotential η, we obtain a peak in the current every time an electronic state lies within the tunneling range of energy between the two Fermi levels. A few examples are seen in Fig. 2.8. The redox level always gives a peak near $\eta = 0$, and for the parameters chosen we see a second peak near ϵ_1^0. When these two energies lie close, one peak may appear as a shoulder. Note that the curves for $\epsilon_1^0 = \pm 0.5$ eV in the figure are not quite symmetric, because the bias breaks the symmetry. In theory, we could expect to see up to three peaks in these curves corresponding to the three molecular orbitals formed, but these only occur for a very strong coupling

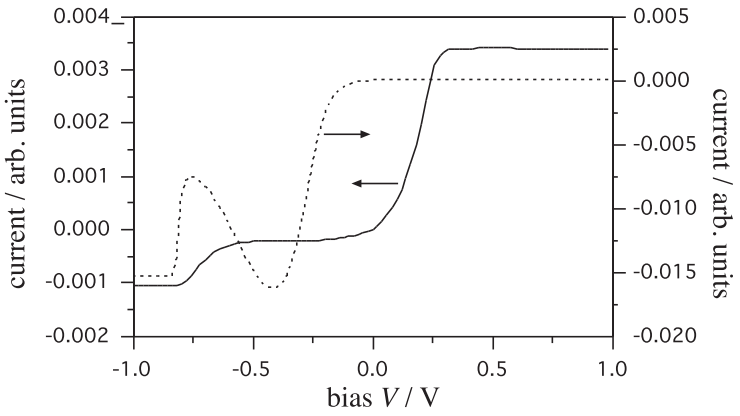

Figure 2.7: Current-potential curves for small coupling to the leads. System parameters: $\Delta = 0.1$ eV, $\epsilon_r = 0.5$ eV, $v = 0.1$ eV, $\epsilon_1 = -0.2$ eV (left curve) and $\epsilon_1 = 0.3$ eV (right curve).

v and small energies of reorganisation. Otherwise the splitting induced by v is hidden under the peak for ϵ_1.

2.4 Conclusions

In this work we have presented a model for the conductivity of a molecular wire containing a redox system, and embedded in an electrochemical environment. We considered the interaction of the redox system with a classical solvent, whose state was represented by a solvent coordinate q in the spirit of the Marcus theory. Using the wide-band approximation, we were able to derive an exact expression for the quantum conductance of a chain of arbitrary length. The thermal average over the solvent configurations had to be performed numerically.

Explicit calculations have been performed for a chain of three atoms. When the electronic levels of the neighboring atoms interact weakly with the redox couple – because their energies are very different or the coupling is weak – the wire behaves much like a single intervening atoms. Interesting new features arise when the redox couple interacts strongly with the neighboring levels. Since the redox level fluctuates with the solvent,

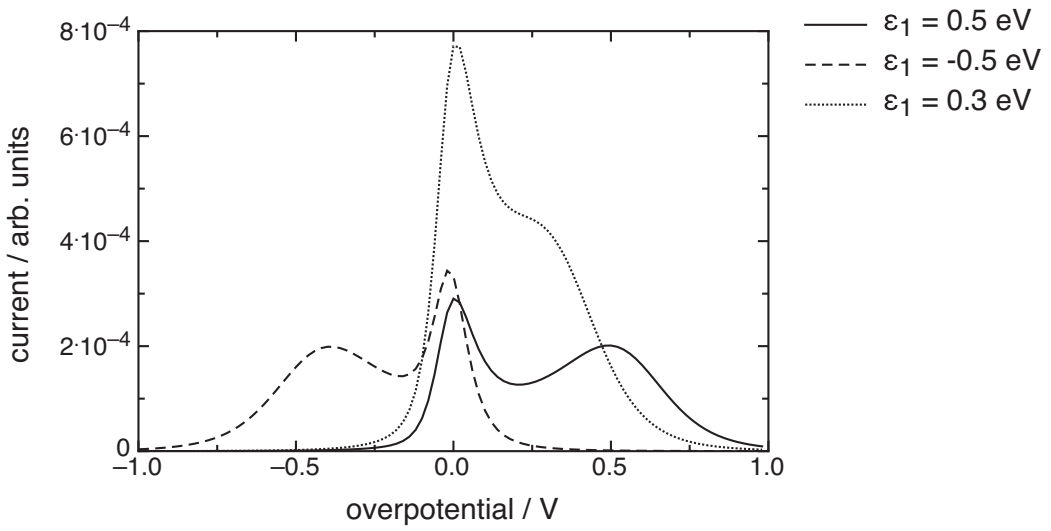

Figure 2.8: Current at constant bias $V = 0.1$ V as a function of the overpotential η for various values of ϵ_1^0, the value of ϵ_1 for vanishing overpotential; $v = 0.1$ eV.

this interaction is dynamic and changes with the solvent configuration.

In an electrochemical environment two potential differences, the bias and the electrochemical potential of the wire, can be varied independently. This makes it possible to perform electronic spectroscopy at constant bias by changing the electrochemical potential. Intermediate states show up as characteristic current peaks.

Our treatment has been limited to a redox couple interacting with a classical solvent. An extension to the case where quantum modes couple to the electron transfer should be possible, using Green's function techniques that have been applied to the case of a single atom [136]. This could give rise to additional structure in current-potential curves.

Chapter 3

Electron Transfer rate between a electrode and a bridged redox

3.1 Introduction

Electron transfer at molecular levels and especially, between chemically active species has been an important and interesting field of active research for a couple of decades [151, 84, 152, 153]. A typical quantity of interest in chemistry is the rate of transfer between two chemiactive species, that is, between donor and acceptor, which in general are solvated. Additionally, with the advent of nanotechnology and molecular electronics, understanding electron transfer rate in molecular chains became a key theoretical interest. A general setup in molecular electron transfer is to study, both in theory as well as in actual experiment, the current-voltage response obtained on passing current between two molecular mesoscopic junctions connected by a single long molecule or a chain of repeated molecular or atomic units. The important quantity of interest in the above scenario is the molecular conduction. The problem of obtaining the conduction of a such a system is well studied one. Formal expressions and relationships like the landauer formula [154, 155, 156] and it's several variants are available to calculate the conductance of such systems [157, 78, 147, 158]. Since conductance is due to transfer of electrons, the question of relationship between conductance and electron transfer rate was answered by A. Nitzan and co-workers [159, 17]. Nitzan derived a relationship between electron transfer rate (κ) and conductance at certain regime.

The rate expression for electron transfer has been derived by several methods, the earliest dating back to the super-exchange method proposed initially by McConnell [59, 148, 160, 161, 162, 163, 164]. Super-exchange treatment is a viable method when the transfer mechanism is tunneling dominated. Another plausible mechanism for transfer is sequential hopping. Typical cases of sequential hopping occurs when there are asymmetries or irregularities in the bridge connecting the acceptor and the donor. Under those conditions phase loss can lead to sequential hopping. The interplay between the sequential hopping and tunneling has been addressed by Medvedev and Stuchebrukhov [165]. They obtained the expression for rate by forming a dynamic correlation function of the couplings or the hopping parameter. Alternate methods to arrive at the rate expression include, density matrix formulation of the problem and equation of motion for the reduced quantum system interacting [166, 167, 168, 169, 170, 171].

Our present work focuses on obtaining an explicit expression for transfer rate in a system where the redox is solvated and is connected by a molecular chain to a electrode. More specifically our attention is concentrated towards obtaining the voltage dependency of the electron transfer rate. As with the previous authors who tackled the problem within the time-dependent fluctuation framework, we assume that at t=0 the electron is in the donor and express the rate of the electron arrival at the final continuum states in the electrode using t-matrix. In this way out treatment of the problem is different from the previous treatments by other authors, wherein the rate expression was derived by expressing the rate as a time dependent correlation function and by partial tracing of the density matrix. It should also be noted that all the earlier works for obtaining transfer rate were mainly oriented towards a DBA system where both the donor and acceptor were either solvated or were continuum of states, while in our system considered only the donor is solvated while the acceptor is an electrode.

3.2 Model and Calculation

The following Hamiltonian is considered as a model for a system of n-sites (each having a single energy level ϵ_i) connecting a reservoir or electrode with energy levels ϵ_k to a redox couple with energy level ϵ_r. The electrode and the redox is connected to the n-site chain through the 1st and nth site respectively. The Hamiltonian is a tight binding model Hamiltonian with additional interactions arising from the redox with the polarization modes. This is achieved by treating these polarization modes as classical oscillator modes. For ease of clarity the Hamiltonian can be split into three parts H_{el}, H_{chain} and H_{ph}, where the H_{el} refers to the electrode part of the Hamiltonian , H_{chain} represents the tight-binding Hamiltonian of the chain + redox couple and the H_{ph} is the used for modelling the classical polarization modes.

$$\mathrm{H}_{el} = \Sigma_k \epsilon_k n_k + \Sigma_k [\bar{\upsilon}_{k1} c_k^\dagger c_1 + h.c] \tag{3.1}$$

$$\mathrm{H}_{ph} = \Sigma_\nu \frac{1}{2} \hbar \omega_\nu q_\nu^2 \tag{3.2}$$

$$\mathrm{H}_{chain} = \sum_{i=1,N} \epsilon_i n_i + \sum_i \{\upsilon_i c_i^\dagger c_{i+1} + h.c\} + (\epsilon_r + \sum_\nu \hbar \omega_\nu g_\nu q_\nu) n_r + \{\bar{\upsilon}_{nr} c_n^\dagger c_r + h.c\} \tag{3.3}$$

It is clear that the matrix form for the H_{chain} is a n+1 $\times$ n+1 tridiagonal matrix with only non-zero entries along the main diagonal and sub-diagonals. For completeness we also give below the matrix form of this Hamiltonian

$$\mathrm{H}_{chain} = \begin{pmatrix} \epsilon_1 & \upsilon & \dots & 0 & 0 \\ \upsilon & \epsilon_2 & \upsilon & \dots & 0 \\ \dots & \dots & \dots & \upsilon & 0 \\ 0 & \dots & \upsilon & \epsilon_N & \bar{\upsilon}_{rn} \\ 0 & \dots & \dots & \bar{\upsilon}_{nr} & \epsilon_r + \sum_\nu \hbar \omega_\nu g_\nu q_\nu \end{pmatrix} \tag{3.4}$$

$$\mathrm{H} = \mathrm{H}_{el} + \mathrm{H}_{chain} + \mathrm{H}_{ph} \tag{3.5}$$

To get the current, the formalism of Ratner et al is employed. Thus the procedure is to get the rate for the transition from redox (r) to the electrode (k) under the influence of voltage W and then perform a thermal averaging of the transition rate. The transition

rate is

$$\text{rate} = \frac{2\pi}{\hbar}\Sigma_k[1 - f(\epsilon - eW)] \mid \mathrm{T}_{kr} \mid^2 \delta(\epsilon_r + \Sigma_\nu \hbar g_\nu q_\nu - \epsilon_k) \tag{3.6}$$

$$\mathrm{T}_{kr} = \bar{\upsilon}_{k1}\mathrm{G}_{1n}\bar{\upsilon}_{nr} \tag{3.7}$$

$$\mathrm{G}^0_{1n} = \frac{(-\upsilon)^{n-1}}{\mathrm{detH}_{chain}} \tag{3.8}$$

The G^0_{1n} is calculated based on the following crucial observation. Let d_n denote the determinant of n x n matrix consisting of ϵ in the diagonal elements and υ in the upper and lower sub-diagonal and the rest of the elements of the matrix being zero.

$$\begin{pmatrix} d_n \\ d_{n-1} \end{pmatrix} = \begin{pmatrix} \epsilon & -\upsilon^2 \\ 1 & 0 \end{pmatrix} \begin{pmatrix} d_{n-1} \\ d_{n-2} \end{pmatrix} \tag{3.9}$$

By repeated application of the above recursion relation, and noting that $d_0 = 1$ and $d_1 = \epsilon$ one arrives at the following result

$$d_n = \frac{\lambda_1^{n+1} - \lambda_2^{n+1}}{\lambda_1 - \lambda_2} \tag{3.10}$$

$$\lambda_{1,2} = \frac{\epsilon \pm \sqrt{\epsilon^2 - 4\upsilon^2}}{2} \tag{3.11}$$

Employing this result in the present Hamiltonian, yields the below given result for the determinant of H_{chain}

$$\mathrm{detH}_{chain} = d_n + i\Delta d_{n-1} \tag{3.12}$$

Where in the above expression d_n is the same as the one defined above . Care should be taken to note that the ϵ used in the definition of $\lambda_{1,2}$ is to be replaced with $\epsilon - \epsilon_i$. This is done since the quantity of interest is the inverse of $\epsilon\mathrm{I} - \mathrm{H}_{chain}$

In the above expression the Green's function element obtained was of the isolated chain Hamiltonian, but the Green's function element to be employed in the formalism should correspond to the total Hamiltonian. This can be obtained from the isolated chain Hamiltonian's Green's function by resorting to a Dyson equation with the interaction of the electrode and redox treated as a perturbation. The resulting expression is as follows:

$$\mathrm{G}_{1N} = \frac{\mathrm{G}^0_{1N}}{[1 - \mathrm{G}^0_{NN}\bar{v}^2_{nr}\mathrm{G}^0_{rr}][1 - \mathrm{G}^0_{11}\bar{v}^2_{k1}\mathrm{G}^0_{kk}]} \tag{3.13}$$

Where in the above expression the isolated Green's function elements are given by

$$\mathrm{G}^0_{11} = \frac{d_{n-1}}{d_n} \tag{3.14}$$

$$\mathrm{G}^0_{NN} = \frac{d_{n-1} + i\Delta d_{n-2}}{d_n + i\Delta d_{n-1}} \tag{3.15}$$

$$\mathrm{G}^0_{kk} = \frac{1}{\epsilon - \epsilon_k \pm i\delta} \tag{3.16}$$

$$\mathrm{G}^0_{rr} = \frac{1}{\epsilon - \epsilon_r - \Sigma_\nu \hbar\omega_\nu g_\nu q_\nu \pm i\delta} \tag{3.17}$$

Alternatively one can arrive at the expression for the G_{1n} element by considering only the Hamiltonian for the chain, H_{chain} and replacing the effect of the reservoir and redox by the corresponding self-energies.Working within the Wide-Band approximation where the self-energy of the electrode is given by ($-i\Delta$). Both the procedures leads to the expression for G_{1n} as

$$\mathrm{G}_{1n} = \frac{(-\upsilon)^{n-1}}{(d_n + i\Delta d_{n-1}) - \frac{[d_{n-1} + i\Delta d_{n-2}]\bar{v}^2_{nr}}{\epsilon - \epsilon_r - \Sigma_\nu \hbar\omega_\nu g_\nu q_\nu}} \tag{3.18}$$

Where in the above expression wide-band approximation has been employed for the self-energy of the reservoir and the self-energy of the redox is $\frac{\bar{v}^2}{\epsilon - \epsilon_r - \Sigma_\nu \hbar\omega_\nu g_\nu q_\nu}$

The above expression for G_{1n} is to be substituted in the rate expression. The delta function can also be split and hence the rate expression takes the form as shown below

$$\kappa(\epsilon, q_\nu) = \frac{2\pi}{\hbar} \int d\grave{\epsilon} \Sigma_k [1 - f(\epsilon - eW)] \mid \bar{v}_{k1} \mid^2 \delta(\grave{\epsilon} - \epsilon_k) \mid \bar{v}_{nr} \mid^2 \mid G_{1r} \mid^2 \delta(\epsilon_r + \Sigma_\nu \hbar g_\nu q_\nu - \grave{\epsilon}) \tag{3.19}$$

Defining $\pi \mid \bar{v}_{k1} \mid^2 \Sigma_k \delta(\epsilon - \epsilon_k) = \Delta$ the above expression reduces to the form below

$$\kappa(\epsilon, q_\nu) = \frac{2}{\hbar} \Delta [1 - f(\epsilon - eW)] \mid G_{1n} \mid^2 \mid \bar{v}_{nr} \mid^2 \tag{3.20}$$

The ϵ in the above expression refers to the energy at which the electron transfer takes place and hence to get the net current flow it is required to sum all the contributions from different energy windows. This summing of different contributions can be performed by integrating with respect to ϵ. That is a sum over ϵ is replaced with $\int d\epsilon \rho(\epsilon_f)$ where $\rho(\epsilon_f)$ is the density of states at the Fermi-surface of the electrode .

$$\kappa(q_\nu) = \frac{2}{\hbar} \Delta \int d\epsilon \rho(\epsilon_f) [1 - f(\epsilon - eW)] \mid G_{1n} \mid^2 \mid \bar{v}_{nr} \mid^2 \tag{3.21}$$

$$\kappa(q_\nu) = \frac{2}{\hbar} \Delta \rho(\epsilon_f) \int d\epsilon [1 - f(\epsilon - eW)] \mid G_{1n} \mid^2 \mid \bar{v}_{nr} \mid^2 \tag{3.22}$$

It is now required to do thermal averaging which is to integrate the above expression for current over all the polarization modes ,q_ν, with a weighing factor of $exp^{-\beta E}$. Alternatively the same process can be viewed as summing over all possible initial states of the redox with respect to polarization modes with a suitable weighing factor depending on the energy of the polarization modes.

The above expression can be evaluated by employing the single reaction co-ordinated

Q for the polarization modes q_ν. Resorting to single reaction co-ordinate [149] , which in effect can be represented as a change of co-ordinates, the crucial observation is that the introduction of single reaction co-ordinate amounts to replacing $\Sigma_\nu \hbar\omega_\nu g_\nu q_\nu$ by $2\lambda q$ and the quadratic term in the exponential for the thermal average is to be replaced by $\lambda q^2 + 2\lambda q$. Thus the expression for net current takes the form as shown below

$$\kappa = \frac{1}{\mathrm{Z}}\frac{2}{\hbar}\Delta\rho(\epsilon_f)\bar{\upsilon}_{nr} \mid^2 \int d\epsilon[1 - f(\epsilon - eW)] \int dq e^{-\beta(\lambda q^2+2\lambda q)} \mid \mathrm{G}_{1n}(q) \mid^2 | \tag{3.23}$$

$$\mathrm{G}_{1n}(q) = \frac{(-\upsilon)^{n-1}}{(d_n + i\Delta d_{n-1}) - \frac{[d_{n-1}+i\Delta d_{n-2}]\bar{\upsilon}_{nr}^2}{\epsilon-\epsilon_r+2\lambda q}} \tag{3.24}$$

$$\mathrm{Z} = \int dq e^{-\beta(\lambda q^2+2\lambda q)} \tag{3.25}$$

While the partition function Z is an elementary gaussian integral. The innermost dq integral can be evaluated by using partial fractions. For brevity defining $\mathrm{D}_n = d_n + i\Delta d_{n-1}$, the G_{1n} takes a form as below.

$$\mathrm{G}_{1n} = \frac{(-\upsilon)^{n-1}(\epsilon - \epsilon_r + 2\lambda q)}{D_n(\epsilon - \epsilon_r + 2\lambda q) - \bar{\upsilon}^2 D_{n-1}} \tag{3.26}$$

The innermost integral over dq can be explicitly evaluated

$$\begin{aligned} \int dq e^{-\beta(\lambda q^2+2\lambda q)} \mid \mathrm{G}_{1n} \mid^2 \quad &= \quad \frac{(\upsilon)^{2n-2}}{2\lambda}[\mathrm{A}e^{-\beta(\mathrm{Q}_0+2\lambda^2)/4\lambda}(\epsilon - \epsilon_r + \mathrm{Q}_0)^2 \\ &\quad +\mathrm{B}e^{-\beta(\bar{\mathrm{Q}}_0+2\lambda^2)/4\lambda}(\epsilon - \epsilon_r + \bar{\mathrm{Q}}_0)^2] \end{aligned} \tag{3.27}$$

where $\mathrm{A} = \frac{D_n}{\bar{\upsilon}_{nr}^2(D_{n-1}\bar{D}_n - \bar{D}_{n-1}D_n)}$ and $\mathrm{B} = \frac{-\bar{D}_n}{\bar{\upsilon}_{nr}^2(D_{n-1}\bar{D}_n - \bar{D}_{n-1}D_n)}$ and $\bar{\mathrm{Q}}_0$ are complex conjugates of each other. Physically this corresponds to the pole in $\mathrm{G}_{1n}(q)$.

$$\mathrm{Q}_0 = \bar{\upsilon}_{nr}^2 \frac{D_{n-1}}{D_n} - (\epsilon - \epsilon_r) \tag{3.28}$$

$$\mathrm{A} = \frac{D_n}{2i\Delta(d_{n-2}d_n - d_{n-1}d_{n-1})} \tag{3.29}$$

$$\mathrm{B} = \frac{-\bar{D}_n}{2i\Delta(d_{n-2}d_n - d_{n-1}d_{n-1})} \tag{3.30}$$

$$\kappa = \mathrm{K}_1 \int d\epsilon \frac{1 - f(\epsilon - eW)}{2i\Delta(d_{n-2}d_n - d_{n-1}d_{n-1})} [D_n e^{-\beta(\bar{\mathrm{Q}}_0 + 2\lambda)^2/4\lambda} (\bar{v}_{nr}^2 \frac{D_{n-1}}{D_n})^2 - c.c] \tag{3.31}$$

$$\mathrm{K}_1 = \frac{2}{\hbar} \frac{\sqrt{\beta}}{\sqrt{\pi\lambda}} \Delta \mid \bar{v}_{nr} \mid^2 \frac{(v)^{2n-2}}{2} e^{-\beta\lambda} \tag{3.32}$$

The above expression for current can be written in a simplified form by resorting to a step function approximation to $1 - f(\epsilon - eW)$.

$$\kappa = \mathrm{K}_1 \int_{\epsilon_f - W}^{+\infty} \frac{[D_n e^{-\beta(\bar{\mathrm{Q}}_0 + 2\lambda)^2/4\lambda} (\bar{v}_{nr}^2 \frac{D_{n-1}}{D_n})^2 - c.c]}{2i\Delta(d_{n-2}d_n - d_{n-1}d_{n-1})} d\epsilon \tag{3.33}$$

3.3 Results and Discussion

Our main focus of attention in this work is oriented towards explaining the dynamic interaction of the redox with the solvent modes and it's subsequent effect on the transfer rate. The chief reason being the redox energy levels varies with the q and hence even though maxima in the transfer rate is expected when the energy level of the redox is same as the energy level of the bridge, but due to the coupling of the redox with the solvent modes, the value of q coupled with the resonant energy level may not be a thermally favoured one. Thus it's the competition between the energy difference between the redox and the bridge and the probability distribution of the initial state of the redox that brings out certain interesting results which we focus on this part.

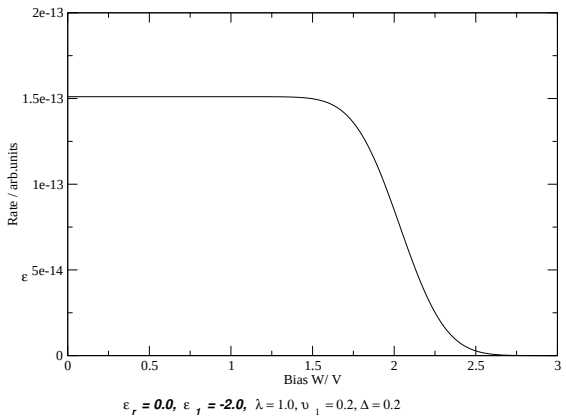

Figure 3.1: Rate Vs. applied Voltage. The energy units are in terms of eV. with the value of the parameters used indicated beneath the graph

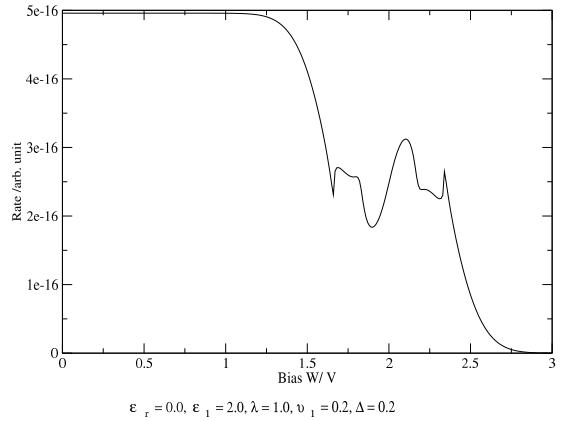

Figure 3.2: Rate Vs. Applied Voltage profile for the case when the relation $\epsilon_1 - \epsilon_r = 2\lambda$ is satisfied. The value of parameters used are shown beneath the graph

Since there exist a number of parameters as input, unless stated specifically, we set the Fermi surface to zero ,$\epsilon_f = 0$, $\Delta = 0.2$ and $\bar{v}_{nr} = v_i$, for all through the rest of the discussion. Fig 3.1. shows the variation of the rate with the applied voltage which could be understood easily from a naive argument as follows: As the applied voltage is increased, the energy levels available in the electrode for the electrons originating from the redox decreases. Thus leading to a rate approaching zero as the voltage is increased. The above is a normally expected behaviour while the interplay between the polarisation modes and the resonance between the redox and the bridge energy levels is clearly visible in Fig 3.2. $q = -1$ corresponds to equilibrium value of the polarization modes when the electron is in the redox and $\epsilon_r - 2\lambda q = \epsilon_i$ is the condition for energy matching between the redox and the bridge. When $\epsilon_i - \epsilon_r = 2\lambda$, the combined effect of thermal averaging and resonant electron transfer is borne out in Fig 3.2.

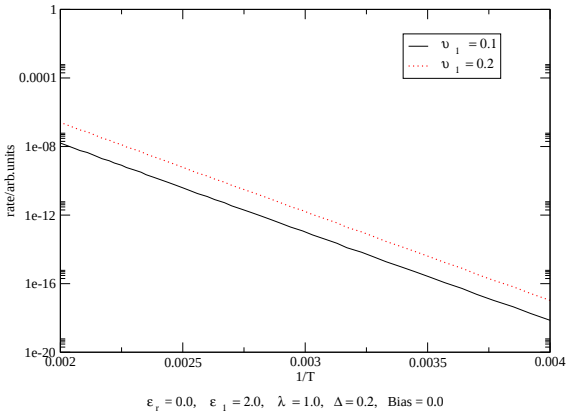

Figure 3.3: Plot for Rate Vs. 1/T at zero bias. The Y-axis is plotted on logarithmic scale. The value of the parameters are used are above.

Fig 3.3 is plotted to show the temperature variation of the rate at zero bias. As expected, the graph shows a linear behaviour when plotted as a function of (1/T). Taking logarithm of the rate equation reveals only three terms dependent on β, apart from uninteresting constant terms. One of the terms is -0.5 log β while the other two terms have linear dependency on β. The contribution from log β become dominant only in the $\beta \to 0$ limit. Since this corresponds to the high temperature limit , for all practical purposes the log variation of rate has a linear dependency on (1/T), a fact borne by Fig

3.3

In order to further investigate the properties of transfer rate at resonance condition, we plot in Fig 3.4. the response of the rate-Voltage for various values of v_1. It is observed from the plots that for small values of the coupling co-efficients , implying a weak bonding between the bridge atoms and between the bridge atoms and the redox, drastic variation from the normal behaviour is not seen. But as the value of v_1 is varied, the observed pattern near the resonance point changes. The changes include a constant transfer rate around a small range of voltage near the voltage value corresponding to the resonance energy, to the rate dropping to zero in some intermediate voltage regime.

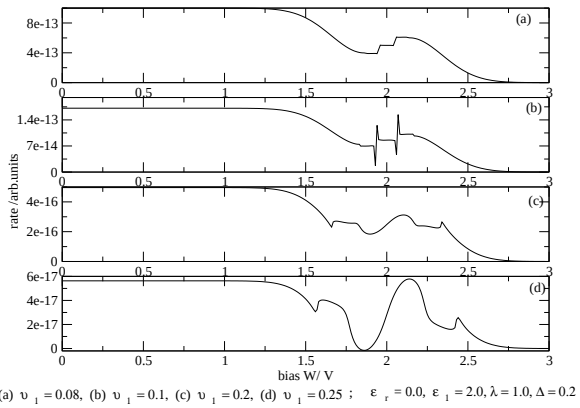

Figure 3.4: Rate Vs. Voltage for different value of v_1

In Fig 3.5. we plot the variation of the rate as a function of the difference in energy between the bridge and the unsolvated redox energy. In particular we wish to highlight the behaviour in the regime where the bridge is situated at a higher energy level than the Fermi level. we first study the variation for a fixed value of λ. The crucial fact to observe is that as long as the bridge is located energetically higher than the Fermi surface, the location of the maximas varies with the actual location of energy level of the bridge and not just only upon the energy difference between the redox and the bridge as one would normally expect. On examining the plots show that the maxima occurs for a fixed value of ϵ_r corresponding to a particular value of λ. Thus in effect while the minima is dependent on the difference between the energy levels, the maxima shows a

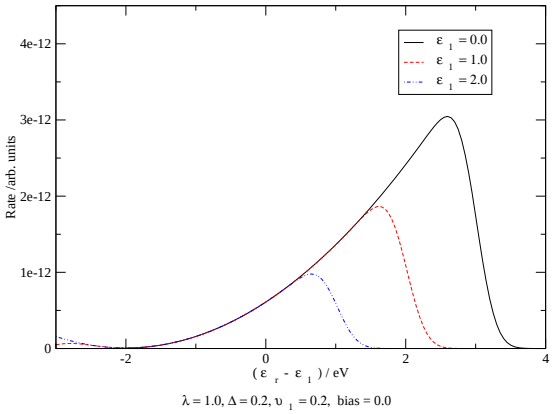

Figure 3.5: Rate Vs. Energy difference between the redox and bridge energies

strong dependency on the solvated energy level of the redox. The effect of λ on the rate profile is shown in Fi

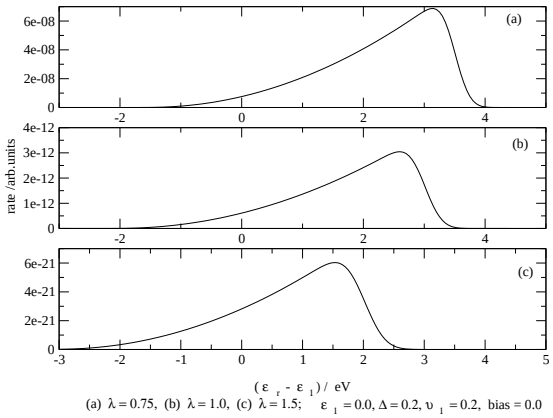

Figure 3.6: Comparison of Rate Vs. Energy difference between the redox and bridge for various value value of re-organisation energy

3.4 conclusion

In this chapter, we have considered a model for electron transfer rate from redox to an electrode via a bridge of N- atoms. The redox considered is allowed to interact with an electrochemical system whose effect in terms of polarization modes are modelled as a bath of classical oscillators with solvent co-ordinates q. We obtained the electron transfer rate from redox to the electrode and have performed an averaging over all possible initial states of the redox. A final voltage dependent expression for the rate is obtained as an integral over all possible energy values available for the incoming electron. This integral has been performed numerically.

We have shown some of the interesting pattern which are otherwise not expected in a heuristic analysis. These pattern in the voltage dependency have been attributed to the competing process namely,resonance tunneling between the redox and the bridge and the solvation of the redox. Additionally we have also shown that by suitable altering the voltage range and the coupling co-efficients it's possible to block the electron transfer in some intermediate voltage ranges. Moreover, the profile of the transfer rate with respect to the energy difference between the bridge and the redox exposes a radically different response due to the effect of intervening solvent modes.

Chapter 4

Electron Transfer Reaction Through an Adsorbed Layer

4.1 Introduction

A proper understanding of electron transfer reaction through an adsorbate intermediate constitutes the first step towards modelling the charge transfer across a chemically modified electrode [172, 173, 174], through a molecular wire [175, 176], or the phenomenon of the molecular electronics [177, 175, 178, 179, 180, 181]. In fact the indirect heterogeneous electron transfer is a recurring feature in all these processes.

In this chapter, the kinetics of an adsorbate mediated electron transfer reaction is considered. The adsorbate is taken to be a metal ion. The reactant is supposed to couple with the adsorbate orbital alone; the direct coupling between the reactant and Bloch states in the metal electrode is neglected. The adsorbate coverage factor θ is allowed to take any arbitrary value in the range $(0, 1)$. Thus starting from a single adsorbate case, corresponding to $\theta \longrightarrow 0$ limit, the formalism remains valid all the way up to a monolayer regime ($\theta = 1$). An important characteristics of metallic adsorbates is that at low coverage, the adsorbate orbital is spatially localized. But in the monolayer regime, one obtains extended electron states in the adlayer. These states form a two-dimensional band [182, 183]. The localized adsorbate state interact strongly with the solvent polarization modes. On the other hand, the interaction of extended electron states with the polarization modes are much weaker, and as a first approximation, it can

be neglected [184] .

A progressive desolvation of adspecies, when the coverage is varied from zero to one, changes adsorbate orbital energy by a few electron volts and hence must leave very significant effects on the electrode kinetics. In addition, in the monolayer regime, the metallic adlayer itself acts as the electrode surface. As a consequence, the adsorbate mediated electron transfer ought to exhibit the characteristics of a direct heterogeneous reaction.

Therefore, a study of how the metallization of an adlayer, and the subsequent desolvation of the adsorbate bridge influences the indirect heterogeneous electron transfer poses a challenging problem in the area of electrode kinetics. In the cited references, the coverage dependent potential energy profile for a bridge mediated electron transfer reactions is generated [184]. In the present chapter, the current-potential relation for such processes is provided and analysed.

The adsorbates exhibit different structural arrangements at different coverage. Even at a fixed coverage, more than one kind of distribution pattern can be observed in the adlayer [185, 186, 187, 188]. Modelling each configuration separately poses a difficult task. Therefore we consider a random distribution of the adsorbates in a two dimensional layer. Subsequently, an 'effective-medium' description is used for the adlayer. This procedure captures the essential features of the adlayer in an average sense [184, 189].

4.2 Model Hamiltonian

An adsorbate has strong electronic coupling with the substrate band states as well as it has electronic overlap with neighbouring adspecies. The latter coupling leads to a two-dimensional band formation in the adlayer at higher coverage. The solvent polarization modes are usually modelled in the harmonic boson approximation and their linear coupling with the adsorbate and reactant lead to solvation and solvent reorganization energies. Here the reactant-adsorbate electronic interation is taken to be weak, thus enabling us to treat it with in the linear response formalism [190]. The model Hamiltonian

representing the physical system is characterized by certain key features to be discussed as follows. Chemisorbed species are distributed randomly on the various adsorption sites on the electrode substrate . Thes sites are considered to form a two-dimensional lattice and are commensurate with underlying substrate. The energy levels associated with the vacant sites are taken to be infinity to ensure that no electron transfer takes place through a vacant site. The random distribution of the adsorbates leads to a randomness in the site energies , that is in a sense, they acquire a random characteristics depending on the occupancy or the vacancy of the site. No randomness is associated with the underlying substrate. Thus the necessary Hamiltonian needed to describe the electron transfer process is shown below [184]

$$\begin{aligned} \mathrm{H} &= \sum_{\sigma} \bar{\epsilon}_r(\{b_\nu + b_\nu^\dagger\}) n_{r\sigma} + \sum_{\sigma} [\upsilon_{ar} c_{a\sigma}^\dagger c_{r\sigma} + h.c] - \sum_{\nu} \lambda_{rc\nu}(b_\nu + b_\nu^\dagger) \\ & \sum_{k,\sigma} \epsilon_k n_{k\sigma} + \sum_{i,\sigma} \hat{\epsilon}_{i\sigma}(\{b_\nu + b_\nu^\dagger\}) n_{i\sigma} + \sum_{\nu} \omega_\nu b_\nu^\dagger b_\nu \\ & + \sum_{k,i,\sigma} [\upsilon_{ik} c_i^\dagger c_k + h.c] + \sum_{i \neq j,\sigma} \upsilon_{ij} c_i^\dagger c_j - \sum_{\{i\},\nu} \lambda_{ic\nu}(b_\nu + b_\nu^\dagger) \end{aligned} \tag{4.1}$$

The redox species labelled r is coupled to adsorbate located at site i=a in the adlayer. The sites in the adlayer are specified by i, while the electrode states are labelled by k. n , $c^\dagger$, c represents the number, creation and annihilation operators for electrons while $b^\dagger$ and b represents the creation and annihilation operators for bosons which model the polarization oscillator modes. ν runs from 1 to 4 labelling the polarization modes corresponding to orientational, vibrational, electronic solvent polarization and surface plasmons respectively and ω_ν represents the associated frequencies. υ is used to denote the coupling strength between the electronic states and λ signifies the strength of adsorbate and redox coupling with the boson modes. The subscripts o and c refers to reactant and adsorbate core.

$$\bar{\epsilon}_r(\{b_\nu + b_\nu^\dagger\}) = \epsilon_r^0 + \sum_{\nu} \lambda_{r\nu}(b_\nu + b_\nu^\dagger) \tag{4.2}$$

$$\hat{\epsilon}_{i\sigma} \equiv \epsilon_{a\sigma}^0 + \sum_{\nu} \lambda_{a\nu}(b_\nu + b_\nu^\dagger) \tag{4.3}$$

ϵ_r^0 and ϵ_a^0 are the energies of redox and adsorbate in gas phase. The expression (4.3) gives the energy of the adsorbate site i when it is occupied. As mentioned before, in case where no adsorbate occupies the site i, the following relation ensures that no charge

transfer takes place through unoccupied sites.

$$\langle \hat{\epsilon}_{i\sigma} \rangle \longrightarrow \infty \tag{4.4}$$

While evaluating the shift in adsorbate orbital energy due to it's coupling to boson, the boson mediated interaction between different sites are neglected. Since only a single species adsorption is considered, a replacement of $\lambda_{i\nu}$ by $\lambda_{a\nu}$ and $\lambda_{ic\nu}$ by $\lambda_{c\nu}$ is followed. Coherent potential approximation is employed to handle the randomness associated with the site energy [189].

4.3 Calculation of current

An examination of the model Hamiltonian shows that, the only possible mechanism for transitions involving redox is provided by the redox-adsorbate coupling terms υ_{ar}. Treating the magnitude of υ_{ar} to be small, the current contribution can be obtained with employing linear response formalism. The microscopic current associated with the electron transfer reaction depends on the average value of the rate of change of electronic occupancy of the redox orbital [190].

$$\mathrm{I} = -e\langle \frac{\partial n_r}{\partial t} \rangle \tag{4.5}$$

$$\mathrm{I} = \frac{e}{\hbar^2} \sum_{\sigma} \int_{-\infty}^{\infty} \langle [V_{I\sigma}^{\dagger}(0), V_{I\sigma}] \rangle dt \tag{4.6}$$

where $V_{I\sigma} = \upsilon_{ar} c_{a\sigma}^{\dagger} c_r$. The first term in the commutator leads to anodic current and the second one gives the cathodic current. The expectation value in the above equation corresponds to a density matrix defined by $\mathrm{H}' = \mathrm{H} - \sum_{\sigma}(V_{Ir}^{\dagger} + V_{Ir})$. Employing Frank-Condon approximation, the anodic current is obtained as

$$\mathrm{I}_A = \frac{e}{\hbar^2} \int_{-\infty}^{\infty} dt \mid V_{ar} \mid^2 \langle \langle c_r^{\dagger}(0) c_r(t) \rangle_F \langle c_{a\sigma}(0) c_{a\sigma}^{\dagger}(t) \rangle_F \rangle_B \tag{4.7}$$

Here $\langle \cdots \rangle_F$ implies an average over electronic degrees of freedom, keeping the bosonic variables as fixed parameters and $\langle \cdots \rangle_B$ denotes the thermal average over boson modes

which are treated in classical approximation. The time correlation function involving $c_{a\sigma}, c_{a\sigma}^{\dagger}$ can be expressed in terms of adsorbate Green's function.

$$\langle c_{a\sigma}(0)c_{a\sigma}^{\dagger}(t)\rangle_F = \frac{1}{\pi}\int_{-\infty}^{\infty}(1-f(\epsilon))e^{i\epsilon\tau/\hbar}(\mathrm{Im}G_{ii})_{i=a}d\epsilon \tag{4.8}$$

$$(G_{ii}(\epsilon))_{i=a} = \langle 0 \mid c_{a\sigma}\langle\frac{1}{\epsilon - \mathrm{H}'}\rangle_{c,i=a}c_{a\sigma}^{\dagger} \mid 0\rangle_F \tag{4.9}$$

$$\langle c_r^{\dagger}(0)c_r(t)\rangle_F = \frac{1}{\pi}\int_{-\infty}^{\infty}e^{-i\epsilon\tau/hbar}\delta(\epsilon-\epsilon_r)d\epsilon \tag{4.10}$$

From the expression (4.9) , it is clear that G_{ii} involves a restricted configuration average denoted by $\langle\cdots\rangle_{c,i=a}$. This implies that while obtaining the configuration average, the site a, which is occupied by an adsorbate and through which the electron transfer takes place, is excluded from the averaging. The occupancy status of the remaining sites are still unspecified. Hence for obtaining the deterministic expression for current, coherent potential approximation is employed. From a physical point of view, this formalism implies that the random adsorbate layer has been replaced by an effective medium and the net effect is one in which a redox is coupled to an adsorbate occupying the site a, and this particular adsorbate is embedded in a two dimensional effective medium.

4.3.1 Estimation of Coherent Potential

As mentioned earlier the randomness inherent in the adsorbate occupancy is handled using coherent potential approximation . Accordingly, the inherent random energy operator $\hat{\epsilon}_{i\sigma}n_{i\sigma}$ in (4.3) is to be replaced by a deterministic operator $k_\sigma n_{i\sigma}$. The coherent potential $k_\sigma(\epsilon)$ is same for all the sites, but depends on the energy variable ϵ. k_σ is determined self-consistently. The required self-consistent equation can be obtained as follows.

$$G_{ij} = G_{ij}^0\delta_{ij} + \sum_l G_{ii}^0 W_{il}G_{lj} \tag{4.11}$$

$$W_{il} = V_{il} + \sum_k \frac{V_{ik}V_{kl}}{\epsilon - \epsilon_k} \tag{4.12}$$

The above equation is obeyed by all GF matrix elements corresponding to sites on two-dimensional lattice. The use of coherent potential for configuration averaging leads to the following result for configuration averaged GF

$$\bar{G} = \frac{1}{\epsilon - W - K(\epsilon)} = \frac{1}{N_{||}} \sum_{u} \frac{1}{\epsilon - k - W(\epsilon, u)} \tag{4.13}$$

The coherent potential operator K has an energy dependency and is deterministic, moreover, it is diagonal in the site basis $\{i\}$, that is $K(\epsilon) = \sum_i k(\epsilon) c_i^{\dagger} c_i$. $N_{||}$ is the number of sites and the summation is over the first brillouin zone. The self-consistent expression for K in the more general context when the energy associated with the vacant site is assumed to be some large ϵ_v but not infinite

$$\frac{\theta}{(\epsilon_a - k)^{-1} - \bar{G}_{ii}} + \frac{(1-\theta)}{(\epsilon_v - k)^{-1} - \bar{G}_{ii}} = 0 \tag{4.14}$$

which in the limit of $\epsilon_v \longrightarrow \infty$ becomes

$$k = \epsilon_a - \frac{1-\theta}{\bar{G}_{ii}} \tag{4.15}$$

Substitution of (4.13) in (4.15) leads to the desired form of self-consistent equation to be used for determining $k_\sigma(\epsilon)$.

$$\bar{G}_{ii} = \frac{1}{N_{||}} \sum_{u} \frac{1}{\epsilon - k_\sigma(\epsilon) - W} = \frac{1-\theta}{\epsilon_{a\sigma} - k_\sigma(\epsilon)} \tag{4.16}$$

The above self-consisten expression for the evaluation of k_σ is exact but requires a tedious summations over the brillouin zone and metal states. These can be further simplified by following the certain assumptions. The assumptions are as follows: (i) The separability of the metal state energy ϵ_k in the direction parallel and perpendicular to the surface. (ii) The substrate density of states in the direction perpendicular to the surface is taken to be Lorentzian, whereas the same is assumed to be rectangular along the surface. (iii) The adsorbate occupies the 'on-top' position on the electrode and is predominantly coupled to the underlying substrate atom. Consequently (4.16) becomes

$$\begin{aligned} \bar{G}_{ii} &= \frac{1-\theta}{\epsilon_{a\sigma} - k_\sigma(\epsilon)} \\ &= \frac{1}{2\Delta_{||}(B-A)\mu} [(A-C) ln \left(\frac{A - \Delta_{||}}{A + \Delta_{||}} \right) - (B-C) ln \left(\frac{B - \Delta_{||}}{B + \Delta_{||}} \right)] \end{aligned} \tag{4.17}$$

$$A/B = \frac{1}{2}[(C+D) \pm \{(C+D)^2 - 4(CD - \frac{\upsilon^2}{\mu})\}^{1/2}] \tag{4.18}$$

$$C = \frac{\epsilon - k_\sigma(\epsilon)}{\mu} \quad ; \quad D = \epsilon - i\Delta_\perp \quad ; \quad \mu = \theta\delta/\Delta_{||} \tag{4.19}$$

δ is the half-bandwidth of the adsorbate monolayer and $2\Delta_{||}$ is the substrate bandwidth at the surface. It should be noted that when the coverage tends to zero the cocnfigurational averaged GF equals θ times the adsorbate GF obtained for the "lone adsorbate" case. Moreover, it can be proven that eventhough μ tends to zero when θ approached zero, the $\bar{G}_{ii}$ remains finite in this limit. This can be verified either by suitable expansion of adsorbate GF, or by a priori taking μ to be zero and reevaluating the adsorbate Green's function. The restricted configurational averaged GF $(G_{ii})_{i=a}$ can be related to the complete configuration averaged GF as

$$(G_{ii})_{i=a} = \frac{1}{(\bar{G}_{ii})^{-1} + k_\sigma - \hat{\epsilon}_{a\sigma}} \tag{4.20}$$

Expressing

$$\bar{G}_{ii}^{-1}(\epsilon,\theta) + K_\sigma(\epsilon,\theta) = X_1(\epsilon,\theta) + iX_2(\epsilon,\theta) \tag{4.21}$$

$$\mathrm{Im}(G_{ii})_{i=a} = \frac{-X_2(\epsilon,\theta)}{[(X_1(\epsilon,\theta) - \hat{\epsilon}_{a\sigma})^2 + (X_2(\epsilon,\theta))^2]} \tag{4.22}$$

In order to evaluate the anodic current I_A, a thermal average over boson modes is to be carried out. Treating them as oscillators in seperate thermal equilibrium, the required density matrix for this average in this limit is

$$\mathrm{P}_{q_\nu} = W(q_\nu) / \int_{-\infty}^{\infty} W(q_\nu) dq_\nu \tag{4.23}$$

$$W(q_\nu) = exp[-\beta \sum_\nu \frac{\omega_\nu}{2}(p_\nu^2 + q_\nu^2) + \bar{\lambda}_\nu q_\nu] \tag{4.24}$$

With the above defined probability function the net expression for anodic current is shown below

$$
\begin{aligned}
I_a &= e\langle n_r\rangle \mid v_{ar} \mid^2 \frac{1}{\sqrt{\pi}\hbar}\frac{1}{\mathrm{Z}}\int d\epsilon \int (\Pi_\nu dq_\nu)\int dt \int d\tau[(1-f(\epsilon)] \\
& exp[-\beta \sum_{\nu=1,2}\frac{\omega_\nu}{2}(p_\nu^2+q_\nu^2)+\bar{\lambda}_\nu q_\nu] \quad exp[i(\epsilon-\epsilon_r-\sum_\nu \lambda_{r\nu}q_\nu)t] \\
& exp[i(X_1(\epsilon,\theta)-\epsilon_a-\sum_\nu \lambda_{a\nu}q_\nu)\tau- \mid X_2(\epsilon,\theta) \mid\mid \tau \mid]
\end{aligned} \tag{4.25}
$$

where

$$
\mathrm{Z} = \int (\Pi_\nu dq_\nu) e^{[-\beta\sum_\nu \frac{\omega_\nu}{2}(p_\nu^2+q_\nu^2)+\bar{\lambda}_\nu q_\nu]} \tag{4.26}
$$

In the above expressions $\bar{\lambda}_\nu = \lambda_{c\nu} + \lambda_{o\nu} + \lambda_{r\nu}$ as the consideration is towards anodic current. A similar expression can be obtained for cathodic current following the same prescription as above. The crucial difference to notice between the anodic and cathodic current is that for cathodic current the $1-f(\epsilon)$ is to be replaced with $f(\epsilon)$ and $\bar{\lambda}_\nu$ for cathodic current is equal to $\lambda_{c\nu}+\lambda_{o\nu}+\lambda_{a\nu}$.

4.3.2 Current expression in terms of re-orangisation energies and overpotentials

Carrying out the various integrations involved in (4.25) the anodic current contribution within the limit of linear response formalism is obtained

$$
I_a \;=\; 2\,e\theta|v_{ar}|^2\sqrt{\pi}\hbar^{-1}\int_{-\infty}^{\infty} sgn(X_2(\epsilon,\theta))\,(1-f(\epsilon))\;\rho_a^{\mathbf{an}}(\epsilon)\,\rho_r^{\mathbf{an}}(\epsilon)d\epsilon \tag{4.27}
$$

Here ϵ_f denotes the electrochemical potential of the system. $\rho_a^{\mathbf{an}}(\epsilon)$ and and $\rho_r^{\mathbf{an}}(\epsilon)$ are the adsorbate and the reactant density of states.

$$
\rho_a^{an}(\epsilon) \;=\; \frac{1}{2\sqrt{\pi P}} Re(w(z)) \tag{4.28}
$$

$$
w(z) \;=\; e^{-z^2} erfc(-iz) \tag{4.29}
$$

$$P = \frac{(4E_a^r E_r^r - (E_{ar}^r)^2)}{4\beta E_r^r} \tag{4.30}$$

$$Z = (-Q^{\mathbf{an}} + i|X_2(\epsilon,\theta)|)/(2\sqrt{P})\,, \tag{4.31}$$

$$Q^{an} = X_1(\epsilon,\theta) - \epsilon_{a\sigma}^0 + \sum_\nu \frac{\lambda_{a\nu}\bar{\lambda}_\nu}{\omega_\nu} - \frac{(\epsilon - \epsilon_r^0 + \sum_\nu \frac{\lambda_{r\nu}\bar{\lambda}_\nu}{\omega_\nu})E_{ar}^r}{2E_r^r} \tag{4.32}$$

in case of anodic current.

$$E_r^r = \sum_\nu \frac{\lambda_{r\nu}^2}{\omega_\nu};\quad E_a^r = \sum_\nu \frac{\lambda_{a\nu}^2}{\omega_\nu};\quad E_{ar}^r = 2\sum_\nu \frac{\lambda_{r\nu}\lambda_{a\nu}}{\omega_\nu}; \tag{4.33}$$

are the reorganization energy for the reactant, adsorbate, and the cross reorganization energy, respectively.

$$\rho_r(\epsilon) = \sqrt{\frac{\beta}{4\pi E_r}}\, exp\left[-\beta\frac{(\epsilon - \epsilon_r')^2}{4E_r}\right] \tag{4.34}$$

Alternatively, we can also write

$$\epsilon_r' = \epsilon_r^0 - \sum_\nu \frac{\lambda_{r\nu}\bar{\lambda}_\nu}{\omega_\nu} = F_R^r - F_O^r - E_r^r \equiv \eta - E_r^r \tag{4.35}$$

where

$$F_R^r = \epsilon_R - \sum_{\nu=1}^4 \frac{\lambda_{R\nu}^2}{\omega_\nu} - 2\sum_{\nu=1}^4 \frac{\lambda_{R\nu}\lambda_{c\nu}}{\omega_\nu} \tag{4.36}$$

$$F_O^r = \epsilon_O - \sum_{\nu=1}^4 \frac{\lambda_{o\nu}^2}{\omega_\nu} - 2\sum_{\nu=1}^4 \frac{\lambda_{o\nu}\lambda_{c\nu}}{\omega_\nu} \tag{4.37}$$

F_O and F_R denote the free energies of the redox-couple in the oxidized and reduced states. $\epsilon_R - \epsilon_O = \epsilon_r^o$, $\lambda_{R\nu} = \lambda_{r\nu} - \lambda_{o\nu}$. Thus $F_R - F_O$ gives the overpotential η for the electron transfer reaction. Similarly, the fraction of overpotential drop between the electrode and adsorbate is related to the change in the adsorbate free energy during the reaction

$$\epsilon_{a\sigma}' = \epsilon_{a\sigma}^0 - \sum_\nu \frac{\lambda_{a\nu}\bar{\lambda}_\nu}{\omega_\nu} = F_R^a - F_O^a - E_a^r \equiv \alpha\eta - E_a^r + E_{ar}^r \tag{4.38}$$

Rewriting the anodic current expression in terms of overpotential, the expression for Q^{an} and ρ_r^{an} takes the form as shown below.

$$Q^{an} \;=\; X_1(\epsilon,\theta) - \alpha\eta - E_a^r + E_{ar}^r - \frac{(\epsilon - \eta + E_r^r)E_{ar}^r}{2E_r^r} \tag{4.39}$$

$$\rho_r^{an}(\epsilon) == \sqrt{\frac{\beta}{4\pi E_r^r}}\, exp\left[-\beta\frac{(\epsilon - \eta + E_r^r)^2}{4E_r^r}\right] \tag{4.40}$$

Proceeding along similar lines of argument for the cathodic current, and noting that $\bar{\lambda}_\nu = \lambda_{c\nu} + \lambda_{o\nu} + \lambda_{a\nu}$ for cathodic current, the expression for Q and ρ_r obtained as shown below,

$$\mathrm{I}_c \;=\; 2\,e\theta|v_{ar}|^2\sqrt{\pi}\hbar^{-1}\int_{-\infty}^{\infty} sgn(X_2(\epsilon,\theta))\, f(\epsilon)\;\rho_a(\epsilon)\,\rho_r(\epsilon)d\epsilon \tag{4.41}$$

$$Q^{cat} \;=\; X_1(\epsilon,\theta) - \alpha\eta + E_a^r - \frac{(\epsilon - \eta - E_r^r + E_{ar}^a)E_{ar}^r}{2E_r^r} \tag{4.42}$$

$$\rho_r^{cat}(\epsilon) == \sqrt{\frac{\beta}{4\pi E_r^r}}\, exp\left[-\beta\frac{(\epsilon - \eta - E_r^r + E_{ar}^r)^2}{4E_r^r}\right] \tag{4.43}$$

The coupling constants between adsorbate and various oscillator modes are scaled by a factor $\sqrt{(1-\theta^2)}$ to take into account the disolvation effect as adlayer itself exhibits metallic properties in the higher coverage regime. Consequently, the solvation and re-organization energy for the adsorbate get scaled by a factor $(1-\theta^2)$, and the solvent induced cross energy terms are scaled as $\sqrt{(1-\theta^2)}$. No such scaling is present for solvation and reorganization energies of the redox-couple. Thus the scaling laws for the various re-organisation are as follows

$$E_{ar}^r(\theta) = \sqrt{(1-\theta^2)}E_{ar}^r(0) \quad ; \quad E_a^r(\theta) = (1-\theta^2)E_a^r(0) \tag{4.44}$$

4.4 Numerical Results and Discussions

The basic concern of this chapter is towards current-overpotential characteristics with

specific emphasis on the variation with the coverage factor (θ) and the fraction of overpotential drop ($\alpha\eta$) across the adsorbate. A first look at the expression for anodic current eq. 4.27 shows that the current is an overlap integral of three terms corresponding to the availability of vacant energy level at the electrode ($1 - f(\epsilon)$), the density of states of the solvated redox couple ρ_r^{an} and the density of states of the adsorbate ρ_a^{an}. The redox density of states has a Gaussian form in terms of ϵ. The self-consistent evaluation of the coherent potential $k_\sigma(\theta)$ enforces a numerical derivation of the adsorbate density of states. However in the following limiting cases, $k_\sigma(\theta)$ takes the value

$$\lim_{\theta \to 0} k_\sigma = \epsilon - \frac{\epsilon - \epsilon_{a\sigma} - w_{ii}}{\theta} - w_{ii} \tag{4.45}$$

and

$$\lim_{\theta \to 1} k_\sigma = \epsilon_{a\sigma} \tag{4.46}$$

where

$$w_{ii} = \sum_k \frac{|v_{ik}|^2}{\epsilon - \epsilon_k} \tag{4.47}$$

.

Consequently, the adsorbate density of states can be analytically obtained in the limits $\theta \to 0$ and 1. Additionally, $\epsilon'_{a\sigma}$ involved in performing the self-consistent evaluation of the coherent potential takes the value as $\alpha\eta - E_a(\theta) + E_{ar}(\theta)$ for anodic current evaluation and $\alpha\eta + E_a(\theta)$ for cathodic current estimation.

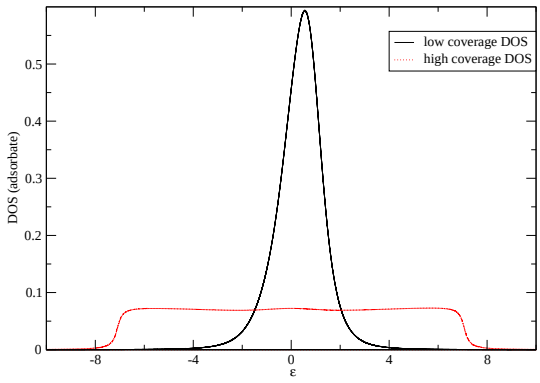

Figure 4.1: Comparison of density of states of the adsorbate for weakly coupled regime at low ($\theta = 0.1$) and high coverage factor ($\theta = 0.9$). The values of parameters (in eV) are as follows: $E_r^r = 0.6, E_{ar}^r(0) = 0.2, E_a^r = 0.4$ and $v = 0.5$ eV.

In what follows, we describe the current vs overpotential profile for different sets of parameters. The adsorbate-electrode interaction is treated both in the weak ($v = 0.5eV$) and strong ($v = 2.0eV$) coupling limits. When the coverage is low, the adsorbate density of states has a single peak Fig. 4.1 . An important consequence of the strong coupling limit is the splitting of the adsorbate level in bonding and anti-bonding states for low θ Fig.4.2. This feature is recaptured in the present analysis since energy dependence of $\Delta(\epsilon)$ is explicitly treated in the present approach On the other hand, the well known wide-band approximation for $\Delta(\epsilon)$ fails to provide the bonding anti-bonding splitting. In the monolayer regime, due to the 2-d bond formation by the adsorbate layer, its density of states acquires a flat profile, irrespective of the strength of the electrode-adsorbate coupling (Fig 4.1, 4.2) . The table I summarizes the values of parameters used in the calculations.

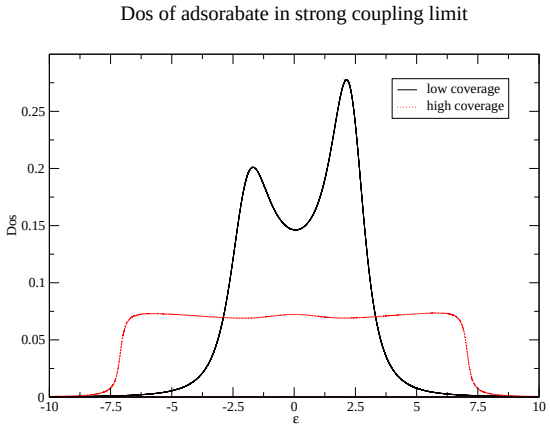

Figure 4.2: Comparison of density of states of adsorbates for strong coupling regime at low and high coverage factor. The values of the various parameters employed (in eV) are as follows: $E_r^r = 1.0, E_{ar}^r(0) = 0.25, E_a^r(0) = 0.75, \Delta_{||} = 1.5, \Delta_{\perp} = 1.5, \mu = 4.5, \upsilon = 2.0$

Table 4.1: Values of parameters used in calculation in eV

	υ	$\Delta_{\|\|}$	$\Delta_{\perp}$	μ	E_r	E_{ar} (0)	E_a (0)
strong	2.0	0.75	1.5	4.5	1.0	0.25	0.75
weak	0.5	0.75	1.5	4.5	0.6	0.2	0.4

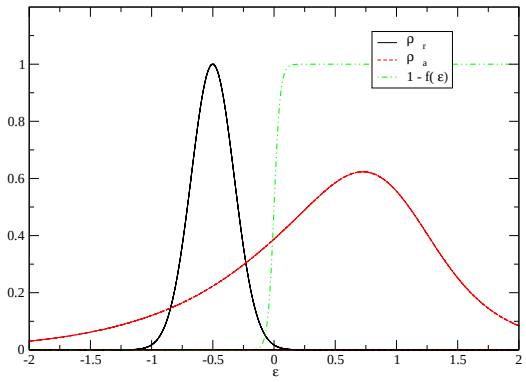

Figure 4.3: Plots showing the density of states for redox, adsorbate and the Fermi distribution for anodic current under zero overpotential. The weakly coupled regime and low coverage of $\theta = 0.3$ is considered here .The values of parameters (in eV) are as follows: $E_r^r = 0.6, E_{ar}^r(0) = 0.2, E_a^r = 0.4$ and $v = 0.5$ eV .

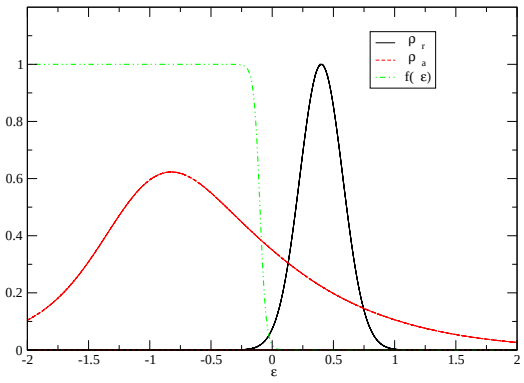

Figure 4.4: Plots showing the density of states for redox, adsorbate and Fermi distribution for cathodic current at zero overpotential. The values of parameters are same as in 4.3

Ideally, under zero overpotential condition, the anodic and cathodic currents are expected to be equal in magnitude. This implies that the profile of the product $\rho_r^{an}(\epsilon)*\rho_a^{an}(\epsilon)$ for anodic current is identical to the product profile $\rho_r^{cat}(\epsilon) * \rho_a^{cat}(\epsilon)$ for the cathodic current. This is a consequence of the equal separation between the peak positions of adsorbate and reactant density of states for anodic and cathodic processes during equilibrium. [Fig. 4.3, 4.4]. The corresponding plots for strongly coupled regime is also shown in Fig. 4.5, 4.6

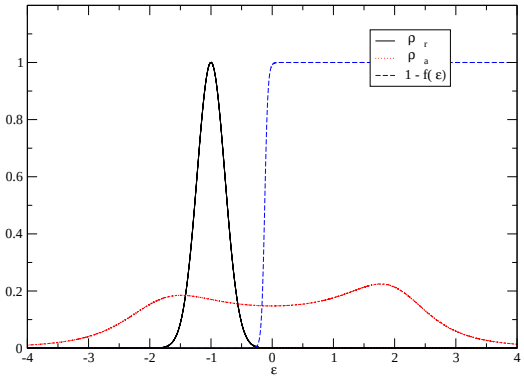

Figure 4.5: Plots showing the density of states for redox, adsorbate and the Fermi distribution for anodic current under zero overpotential. The strongly coupled regime and low coverage of $\theta = 0.3$ is considered here .The values of parameters (in eV) are as follows: $E_r^r = 1.0, E_{ar}^r(0) = 0.25, E_a^r = 0.75$ and $v = 2.0$ eV .

As noted earlier, the electrochemical potential ϵ_f has been set as the zero of energy scale for the direct electron transfer reaction. The presence of additional charge particles for the bridge assisted electron transfer reaction, namely the adsorbates, changes ϕ, the equilibrium potential of the electrode. This is turn gets reflected as a θ dependent variation $\Delta\phi(\theta)$ in $\epsilon_f(\equiv 0)$. The fact that the anodic and cathodic currents at equilibrium potential are identical in magnitude provides a novel method for the determination of $\Delta\phi(\theta)$. Thus the relation $I_a(\eta = 0) = I_c(\eta = 0)$ with $f(\epsilon) = (1 + exp(-\beta(\epsilon + \Delta\phi(\theta)))^{-1}$ (cf eqs. 4.27 and 4.41) enables us to evaluate $\Delta\phi(\theta)$. The variation of $\Delta\phi$ with respect to θ is shown in Fig.4.7 in the limit of weak and strong adsorbate-electrode interaction, with $E_r^r = 0.6$ eV, $E_{ar}^r(0) = 0.2$ eV, $E_a^r\ (0) = 0.4$ eV. The value of $\Delta\phi(\theta)$ depends on the strength of coupling v; its magnitude increases as the coupling becomes stronger.

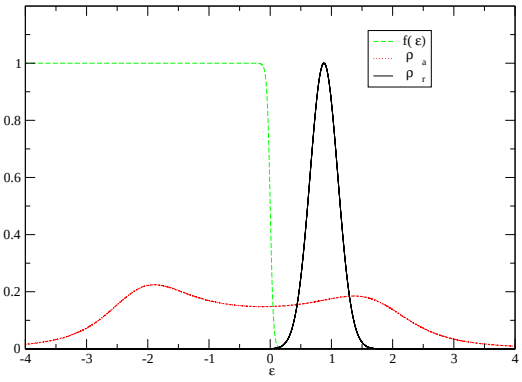

Figure 4.6: Plots showing the density of states for redox, adsorbate and Fermi distribution for cathodic current at zero overpotential. The values of parameters are same as in 4.5

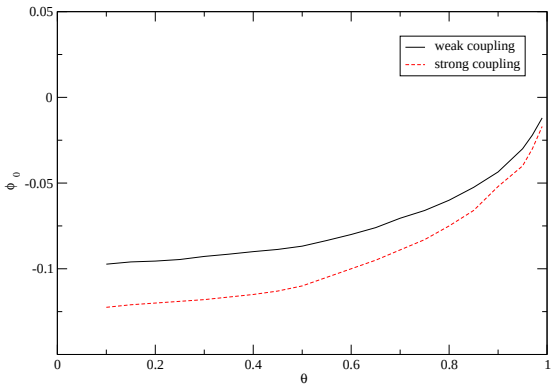

Figure 4.7: Plots showing the variation of $\Delta\phi$ with respect to θ the coverage factor. The values of re-organisation energies employed were same in both the curves. E_r = 0.6 eV, $E_a(0)$ = 0.4 eV, $E_{ar}(0)$ = 0.2 eV

$|\Delta\phi(\theta)|$ is again large for low θ values and remains almost constant in this region. Note that in this regime, the charge on the adsorbate remains localized on the adsorption site. $|\Delta\phi(\theta)|$ starts diminishing sharply for $\theta > 0.6$ and it tends to 0 as $\theta \to 1$. This behaviour is expected. As $\theta \to 1$, the adsorbate layer becomes metallic and gets incorporated in the electrode. The electron transfer acquires the characteristics of a direct heterogeneous reaction, and consequently as noted earlier, the electrochemical potential μ again lies at the zero of the energy scale.

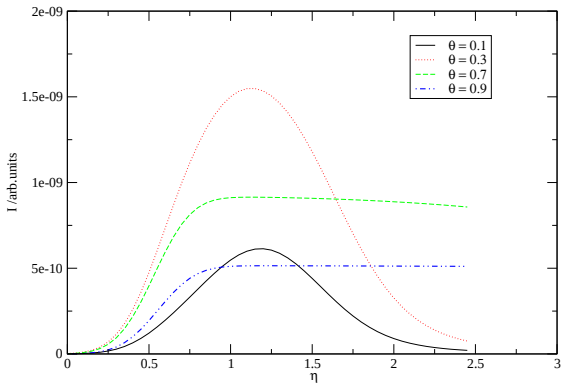

Figure 4.8: anodic current vs η for $\alpha = 0.3$. The values of the various parameters employed (in eV) are as follows: $E_r^r = 1.0, E_{ar}^r(0) = 0.25, E_a^r(0) = 0.75, \Delta_{||} = 1.5, \Delta_\perp = 1.5, \mu = 4.5, \upsilon = 2.0$

We first present the current-overpotential profile in the weak coupling limit ($\upsilon = 0.5\ eV$) for a range of θ and α. The employed values of various reorganization energies are $E_r^r = 0.6$, $E_{ar}^r(0) = 0.2$, $E_a^r\ (0) = 0.4$. The general behaviour can be analysed by looking at the case of lower coverage and high coverage regimes respectively, and then by investigating the effect of variation of α in these limits. Fig. 4.8 shows that for a fixed α, anodic current as well as the current peak height increases with θ in the small θ range ($\theta = 0.1$ and 0.3). This feature arises due to a better overlap between the reactant and adsorbate density of states, whose peak positions are approximately separated by a distance $E_r^r + E_a^r(\theta) - E_{ar}^r(\theta)$. An increase in θ reduces E_a^r and E_{ar}^r (cf eq. 4.44), and hence the peak separation diminishes and the overlap gets enhanced. The presence of anodic current peak at η_p signifies negative differential resistance for $\eta > \eta_p$. This feature

is absent in the higher coverage limit. For large value of θ, the current at higher η exhibits a saturation effect. This is a consequence of the fact that the maximum in the adsorbate density of states ρ_a^{an} is now suppressed. ρ_a^{an} now acquires a plateau profile (Fig 4.1). The plateau height, and therefore the overlap between the reactant and adsorbate density of states decreases with the increasing coverage. Therefore a decrease in the saturation current results as $\theta \to 1$ (curve $\theta = 0.7$ and 0.9 in Fig. 4.8).

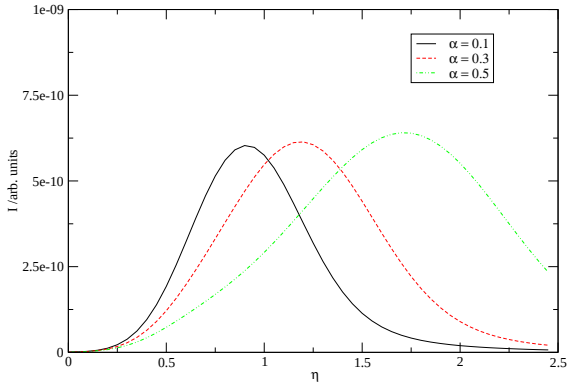

Figure 4.9: anodic current vs η for $\theta = 0.1$ in the weak coupled regime. The values of parameters (in eV) are as follows: $E_r^r = 0.6, E_{ar}^r(0) = 0.2, E_a^r = 0.4$ and $v = 0.5$ eV.

The effect of the α variation on the anodic current is highlighted in Fig. 4.9, 4.10 and 4.11. This effect is more pronounced in the low coverage regime due to the presence of adsorbate density of states peak. The reactant and adsorbate density of states peak separation increases with the increasing α. Consequently, the maximum overlap between the two occurs at larger η. This explains the occurrence of the anodic current peak at higher η values as α increases . On the other hand, the near constant adsorbate density of states for large θ ensures a minimal effect of α variation on the anodic current (Fig. 4.11, 4.12).

Next the strong coupling limit with [$v = 2.0$ eV, $E_r^r = 1.0$ ev, $E_{ar}^r(0) = 0.25$ eV, E_a^r (0) $= 0.75$ ev]is considered. Figures 4.13, 4.14, 4.15 and 4.16 shows the current overpotential response in the strong coupling regime. As in the case of low coverage, the I_a *vrs* η plot exhibits a negative-differential region (Fig. 4.13, 4.14).

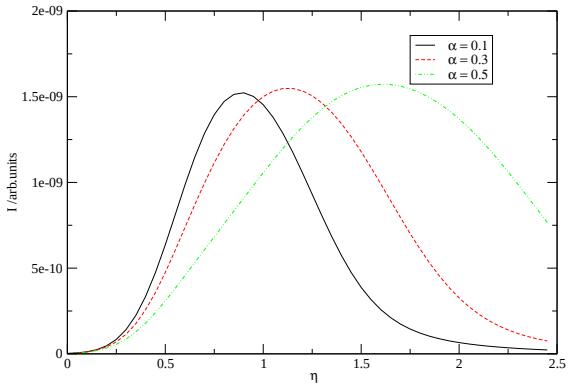

Figure 4.10: anodic current vs η for $\theta = 0.3$ in weak coupled regime. The values of parameters (in eV) are as follows: $E_r^r = 0.6, E_{ar}^r(0) = 0.2, E_a^r = 0.4$ and $v = 0.5$ eV.

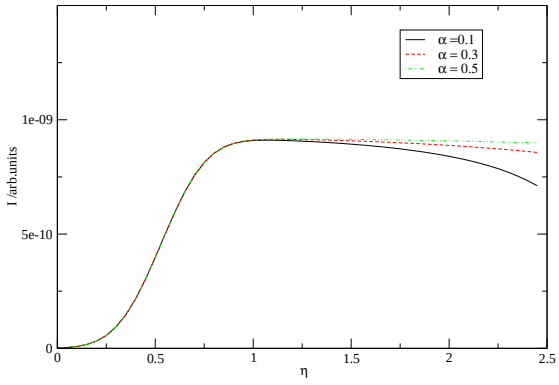

Figure 4.11: anodic current vs η for $\theta = 0.7$. The values of parameters (in eV) are as follows: $E_r^r = 0.6, E_{ar}^r(0) = 0.2, E_a^r = 0.4$ and $v = 0.5$ eV.

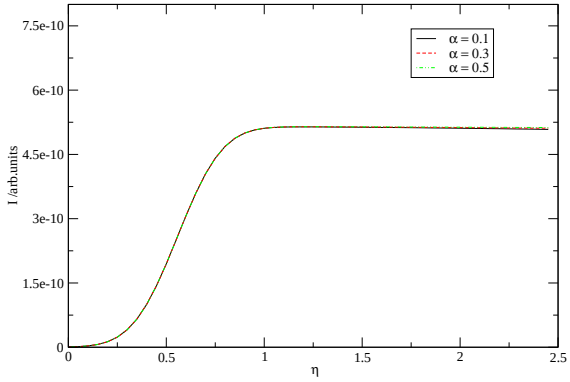

Figure 4.12: anodic current vs η for $\theta = 0.9$. The values of parameters (in eV) are as follows: $E_r^r = 0.6, E_{ar}^r(0) = 0.2, E_a^r = 0.4$ and $v = 0.5$ eV.

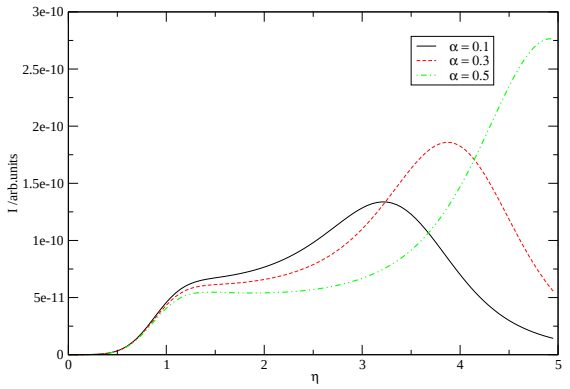

Figure 4.13: anodic current vs η for $\theta = 0.1$. The values of the various parameters employed (in eV) are as follows: $E_r^r = 1.0, E_{ar}^r(0) = 0.25, E_a^r(0) = 0.75, \Delta_{||} = 1.5, \Delta_{\perp} = 1.5, \mu = 4.5, v = 2.0$

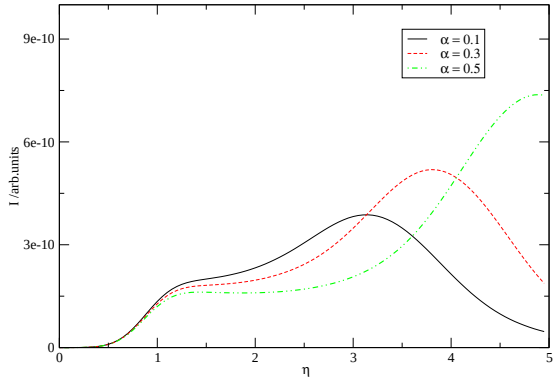

Figure 4.14: anodic current vs η for $\theta = 0.3$.The values of the various parameters employed (in eV) are as follows: $E_r^r = 1.0, E_{ar}^r(0) = 0.25, E_a^r(0) = 0.75, \Delta_{||} = 1.5, \Delta_{\perp} = 1.5, \mu = 4.5, \upsilon = 2.0$

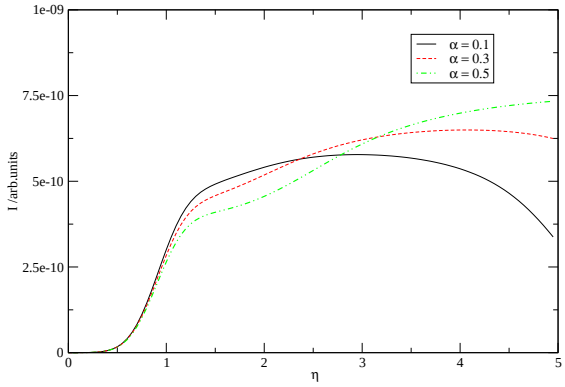

Figure 4.15: anodic current vs η for $\theta = 0.7$. The values of the various parameters employed (in eV) are as follows: $E_r^r = 1.0, E_{ar}^r(0) = 0.25, E_a^r(0) = 0.75, \Delta_{||} = 1.5, \Delta_{\perp} = 1.5, \mu = 4.5, \upsilon = 2.0$

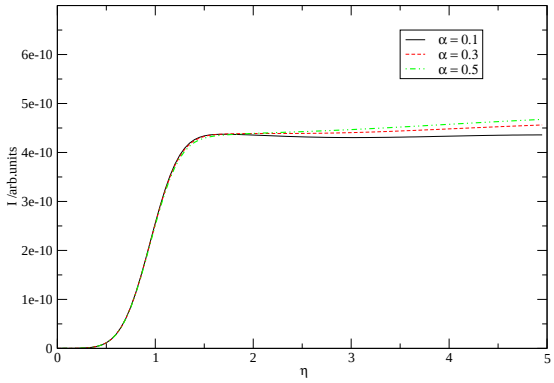

Figure 4.16: anodic current vs η for $\theta = 0.9$. The values of the various parameters employed (in eV) are as follows: $E_r^r = 1.0, E_{ar}^r(0) = 0.25, E_a^r(0) = 0.75, \Delta_{||} = 1.5, \Delta_\perp = 1.5, \mu = 4.5, \upsilon = 2.0$

More importantly, the presence of two peaks in ρ_a^{an} when coupling υ is large and θ is small (Fig. 4.2) leads to a saddle point and a maximum in the I_a vrs. η plot. For the set of parameters currently employed, the $I_{a,Max}$ now occurs at a much larger η in comparison to the weak coupling limit, and may not be accessible experimentally. However, the saddle point in the current appears in an overpotential range where the anodic current peak appears in the weak coupling limit. For large coverage, current potential profile are similar in strong and weak coupling limit. Interestingly, the saturation current is smaller in the large coupling case due to a decrease in the height of ρ_a^{an}. In fact this lowering of the current in the strong coupling holds true for any coverage and η. This is shown in Fig. 4.17 wherein the variation of equilibrium current I^o with respect to coverage is plotted. The I^o is smaller for larger υ, and as explained earlier in the context of Fig. 4.8, shows a maximum in the intermediate coverage regime. However it may be noted that when $\upsilon \to 0$, current would be proportional to $|\upsilon|^2$, and an increase in υ in this very weak coupling limit will lead to an increase in the current.

The high coverage regime of $\theta \to 1$ corresponding to a formation of monolayer of a decrease in the current for higher η when the coverage is low virtually mimics the Marcus inverted region for a homogeneous electron transfer reaction. On the other hand, the current getting saturated at higher η when the coverage is large is also true for a direct

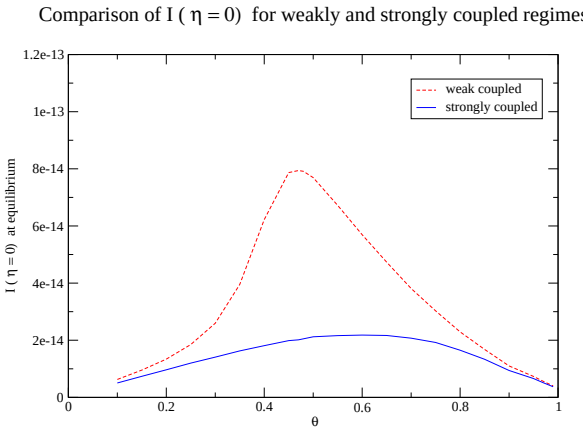

Figure 4.17: Plots showing the equilibrium current at zero overpotential I_0 vs θ for strong and weak coupled regime. The values of re-organisation energies were selected be the same for both the curves, $E_r = 0.6$ eV, $E_a(0) = 0.4$ eV, $E_{ar}(0) = 0.2$ eV

heterogeneous electron transfer reaction. Thus depending on the extent of coverage, an adsorbate mediated electron transfer at an electrode exhibits the characteristics of both homogeneous and heterogeneous electron transfer reactions. The localization of adsorbate electron at low coverage and its delocalization at high coverage is the reason behind this phenomena.

4.5 Summary and Conclusions

In this chapter, we considered electron transfer in an electrochemical system, from a solvated redox to an electrode mediate by intervening adsorbate atoms. Further randomness is introduced in the model in terms of the coverage factor which relates to the number of adsorbate atoms adsorbed on the electrode surface. The theory developed is valid for a range of regime, lone adsorbate mediate transfer to the monolayer formatted direct electron transfer regime. The inherent randomness involved in the adsorbate distribution on the surface has been tackled by coherent potential approximation (CPA) and separate expression are derived for anodic and cathodic current.

Explicit attention was paid to the low coverage and high coverage regime, even though the formalism is valid for all regime, since at these two regions the theory could be compared with pre-existing literature. Plots were also provided for intermediate regimes and additionally, the effect of the adsorbed atoms on the Fermi level of the electrode were incorporated by means of a shifted equilibrium potential $\Delta\phi(\theta)$, ensuring that the anodic and cathodic current were equal under zero overpotential condition.

The analysis also provides a novel method for determining the variation in $\Delta\phi(\theta)$ with changing adsorbate coverage.

The fraction of overpotential drop across the electrode-adsorbate is incorporated and the collective plots are analysed. We have proved that this fraction of overpotential drop plays a significant role in determining the response behaviour of current, typically the location and extent of the maximas in case of lower coverage situations. while in case of high coverage regime, the effect is not profound and the electron transfer follows the traditional direct electron transfer as expected from heuristic arguments.

The dependence of anodic current in the weak and strong electrode-adsorbate coupling is analyzed. In the former case, I_a vrs overpotential profile exhibits a peak, where as in the later case, and in the same overpotential region, the current plot shows a saddle point behaviour. This fact can be used to distinguish a weakly chemisorbed bridge from a strongly chemisorbed one. These distinguishing features occur only when the coverage is low. At high coverage, $I_a \sim \eta$ plots have identical profile for weak and strong coupling cases

At low coverage, it is possible to recover the Marcus inverted region, which is absent when the coverage is large. The localized nature of the adsorbate orbital when coverage is low, and its getting delocalised for high coverages leads to this behaviour.

Chapter 5

Conclusion

The central aim of the thesis is to develop a formal method for understanding electron transport along molecular chains with arbitrary number of units containing embedded redox centers. Thus the whole problem can be studied by concentrating on several sub-categories, each of which are interesting problem in themselves. As mentioned in the introduction, a typical experiment set-up consist of electrodes, chemisorbed species, bridging molecules, redox centers embedded in the bridging units and electrolytes or solvents interacting with the redox. Hence, the problems constituting the sub-categories, in keeping with the various components mentioned above, can be viewed as follows: Obtaining the effect of the redox center on the conductance of the bridging wire and understanding the effect of the adsorbate species on the electron transfer. Chapters 2 and 3, address the first question wherein the conductance of a simple bridging molecular units with a single redox center is calculated along with the I-V profiles. In chapter 2, the results obtained from the analysis of a simple system of two electrodes connected by a molecular wire with redox center was presented. By varying re-organisation energies and coupling strengths, it was shown that interesting features like current rectification, extended plateaus in I-V profile and negative differential resistance can be observed. Additionally, the possibility of such a system to model electronic spectroscopy at constant bias is also mentioned. In chapter 3, the specific case of electron transfer from redox to a single electrode was addressed. An explict expression for the rate of electron transfer, which is voltage dependent, is derived and the effect of altering various energies and coupling strengths is analysed. The results presented shows the effect of competition between resonance dominated tunneling and the solvation of the redox.

The specific question of the effect of the chemisorbed species on the electron transfer is analysed in chapter 4 wherein metallic adsorbates are allowed to settle on the surface of a electrode with different coverages and the formalism derived remains valid from a single adsorbate to a mono-layer regime. The results were compared with the standard results obtained from pre-existing formalism for single adsorbate mediated electron transfer as a limiting case check. As expected heuristically, the low coverage results from the calculations exhibited behaviour as predicted by earlier formalisms developed for handling lone adsorbates. The high coverage results were commensurate with results from direct electron transfer due to a metallization of adlayer. Hence, the derived formalism bridges both the earlier existing formalisms, and is valid for full intermediate regions. The effect of fractional drop in overpotential across the electrode-adsorbate interface is also presented. The significance of this drop in determining the overall nature of the current-voltage profile is also highlighted.

In all the calculations presented so far, the polarisation modes are considered as classical oscillators. An extension of these calculations to quantum modes, is expected to give additional structures in the current-voltage profile. One of the possible interactions which has not been considered is the interaction of molecular electronic junction with radiation field. The radiation field interaction is a plausible and less-expolored candidate for controlling the operation. Optical switching and laser control of such devices are experimentally realised and, even though, the effect of these on conduction properties were experimentally studied, a full theory is yet to be formalised.

Effects of electron-electron interaction and polarization mode anharmonicity remain to be analysed in future works. The presence of stereochemical changes, and its effect on current through molecular junctions, is a potential candidate for further works. This question cannot be dealt at present, because the experimental information available on stereochemical changes brought about by applied bias is substantially limited. With constant advances in experimental capabilities, the above mentioned question will receive the required attention in near future. On a final note, some of the newest experimental areas, like utilizing current in molecular junction to effect chemical transformation, bond breaking and junction heating with associated thermal transport have their theoretical formalism still at a nascent level. These are some of the suitable candidates that require further investigation.

Bibliography

[1] N.J. Tao. Probing potential tuned resonant tunneling through redox molecule with scanning tunneling microscope. *Phys. Rev. Lett*, 76:4066–69, 1996.

[2] G. Moore. Cramming more components onto integrated circuits. *Electronics.*, 38:114, 1965.

[3] A. Aviram(ed). *Molecular Electronics: Science and Technology.* College Park, MD: American Institute of Physics, 1992.

[4] M.R. Bryce M.C. Petty and D. Bloor (ed). *An Introduction to Molecular Electronics.* Oxford: Oxford University Press.

[5] J. Jortner and M. Ratner (ed). *Molecular Electronics.* Oxford: Blackwell Science, 1997.

[6] M. Ratner A. Aviram and V. Mujica (ed). *Molecular Electronics II.* New York: New York Academy of Sciences, 2002.

[7] M. A. Ratner and M.A. Reed. *Encylopedia of Physical Science and Technology.* New York: Academic.

[8] M. A. Reed and T. Lee. *Molecular Nanoelectronics.* Stevenson Raunch, CA: American Scientific Publishers, 2003.

[9] A. Nitzan. Electron transmission through molecules and molecular interface. *Annu. Rev. Phys. Chem.*, 52.

[10] C.A. Mirkin and M.A. Ratner. Molecular electronics. *Annu. Rev. Phys. Chem.*, 43:719–754, 1992.

[11] J.R.Heath and M.A. Ratner. Molecular electronics. *phys. Today.*, 56 (5):43, 2003.

[12] A. Nitzan and M.A. Ratner. Electron transport in molecular wire junctions: Models and mechanisms. *Science.*, 300:1384–1389, 2003.

[13] P. Packan. Pushing the limits. *Science.*, 24:2079–2081, 1999.

[14] J.K. Gimzewski C.Joachim and A.Aviram. Electronics using hybrid-molecular and mono-molecular devices. *Nature.*, 408:541–549, 2000.

[15] R.M.Metzger *et al.* Electrical rectification in a langmuir-blodgett monolayer of dimethyanilinoazafullerene sandwiched between gold electrodes. *J. Phys. Chem. B.*, 107:1021–1027, 2003.

[16] R.A. Marcus. On the theory of oxidation-reduction reactions involving electron transfer. *J. Chem. Phys.*, 24:966–979, 1956.

[17] A. Nitzan. A relationship between electron transfer rates and molecular conduction. *J. Phys. Chem. A.*, 105:2677–2679, 2001.

[18] Z. J. Donhauser *et. al.* Conductance switching in single molecules through conformational changes. *Science.*, 292:2303–7, 2001.

[19] E. G. Emberly and G.Kirczenow. Current driven conformational changes, charging and negative differential resistance in molecular wires. *Phys. Rev. B.*, 64:125318–125323, 2001.

[20] E.G. Emberly and G. Kireczenow. The smallest molecular switch. *Phys. Rev. Lett.*, 91:188301–188305, 2003.

[21] M. Berthe *et. al.* Electron transport via local polarons at interface atoms. *Phys. Rev. Lett.*, 97:206801–4, 2006.

[22] G.V. Nazin X.H. Qiu and W. Ho. Vibrationally resolved fluorescence excited with submolecular precision. *Science*, 299:542–6, 2003.

[23] J.R. Hahn and W. Ho. Imaging and vibrational spectroscopy of single pyridine molecules on ag(110) using low-temperature scanning tunnelling microscope. *J. Chem. Phys.*

[24] J.H. Lee H.J. Lee and W. Ho. Vibronic transitions in single metalporphyrins. *ChemPhysChem*, 6:971–5, 2005.

[25] G.V. Nazin X.H. Qiu and W. Ho. Vibronic states in single molecule electron transport. *Phys. Rev. Lett*, 92:206102–206106, 2004.

[26] J. Tersoff and D.R. Harmann. Theory of scanning tunnelling microscope. *Phys. Rev. B*, 31:805–13, 1985.

[27] J. Park *et. al.* Coulomb blockade and the kondo effect in single-atom transistors. *Nature*, 417:722–5, 2002.

[28] J.M. Tour Z.K. Keane, J.W.Ciszek and D. Natelson. Three-terminal devices to examine single-molecule conductance switching. *Nano. Lett*, 6:1518–21, 2006.

[29] M. Poot *et. al.* Temperature dependence of three-terminal molecular junctions with sulphur endfunctionalized terclohexylidenes. *Nano. Lett*, 6:1031–5, 2006.

[30] P.G. Piva *et al.* Field regulation of single-molecule conductivity by a charged surface atom. *Nature*, 435:658–61, 2005.

[31] J.K. Steach F. Anariba and R.L. McCreery. Strong effects of molecular structure on electron transport in carbon/molecule/metal molecular electronic junctions. *J. Phys. Chem B*, 109:11163–72, 2005.

[32] X. Guo *et. al.* Covalently bridging gaps in single-walled carbon nanotubes with conduction molecules. *Science*, 311:356–9, 2006.

[33] T. Rakshit *et. al.* Silicon-based molecular electronics. *Nano. Lett*, 4:1803–7, 2004.

[34] N.P. Guisinger *et. al.* Room temperature negative differential resistance through individual organic molecules on silicon surfaces. *Nano. Lett*, 4:55–59, 2004.

[35] V. Mujica and M.A. Ratner. Semiconductor/molecule transport juncrions: an analytic form for the self-energies. *Chem. Phys*, 326:197–203, 2006.

[36] X.E.He *et. al.* Discrete conductance switching in conducting polymer wires. *Phys. Rev. B*, 68:045302–8, 2003.

[37] A.J. Ricco E.W. Paul and M.S. Wrighton. Resistance of polyaniline films as a function of electrochemical potential and fabrication of polyaniline based microelectronic devices. *J. Phys. Chem*, 89:1441–1447, 1985.

[38] M. Kruger *et. al.* Electrochemical carbon nanotubes field-effect transistors. *Appl. Phys. Lett*, 78:1291–1294, 2001.

[39] S. Rosenblatt *et. al.* High performance electrolyte gated carbon nanotube transistors. *Nano. Lett*, 2:869–72, 2002.

[40] D.I. Gittins *et. al.* A nanometre-scale electronic switch consisting of a metal cluster and redox-addressable groups. *Nature*, 408:67–69, 2000.

[41] B.Q. Xu *et. al.* Electromechanical and conductance switching properties of single oligothiophene molecules. *Nano. Lett*, 5:1491–95, 2005.

[42] F. Chen *et. al.* A molecular switch based on potential-induced changes of oxidation state. *Nano. lett*, 5:503–506, 2005.

[43] X. Xiao *et. al.* Redox-gated electron transport in electrically wired ferrocene molecules. *Chem. Phys*, 326:138–143, 2006.

[44] N. Tao. Electrochemical fabrication of metallic quantum wires. *Journal of Chemical Education*, 82:720, 2005.

[45] S. Datta. *Electronic Transport in Mesoscopic Systems.* Cambridge: Cambridge Univeristy Press, 1995.

[46] D.M. Newns. Self-consistent model of hydrogen chemisorption. *Phys. Rev*, 178:1123–35, 1969.

[47] S. Datta Y.Xue and M.A. Ratner. Charge transfer and band lineup in molecular electronic devices: A chemical and numerical interpretation. *J. Chem. Phys*, 115:4292–4300, 2001.

[48] A. Roitberg V. Mujica, M.Kemp and M.A. Ratner. Current-voltage characteristics of molecular wires: Eigenvalue staircase, coulomb blockade, and rectification. *J. Chem. Phys*, 104:7296–7306, 1996.

[49] N. S. Hush L. E. Hall, J.R. Reimers and K. Silverbrook. Formalism, analytical model, and a priori green's-function-based calculations of the currentâĂŞvoltage characteristics of molecular wires. *J. Chem. Phys*, 112:1510–1522, 2000.

[50] W. Wenzel G. Schon J. Heurich, J. C. Cuevas. Electrical transport through single-molecule junctions: From molecular orbitals to conduction channels. *Phys. Rev. Lett.*, 88:256803–7, 2003.

[51] A. Nitzan *et. al.* On the electrostatic potential profile in biased molecular wires. *J. Chem. Phys*, 117:10837–10842, 2002.

[52] M. Brandbyge *et. al.* Density-functional method for nonequilibrium electron transport. *Phys. Rev. B*, 65:165401–18, 2002.

[53] J.C. Cuevas *et. al.* Theoretical description of the electrical conduction in atomic and molecular junctions. *Nanotechnology*, 14:29–38, 2003.

[54] E. Scheer *et. al.* Conduction channel transmissions of atomic-size aluminum contacts. *Phys. Rev. Lett.*, 78:3535–8, 1997.

[55] E. Scheer *et. al.* The signature of chemical valence in the electrical conduction through a single-atom contact. *Nature*, 394:154–7, 1998.

[56] H.E. van den Brom and J. M. van Ruitenbeek. Quantum suppression of shot noise in atom-size metallic contacts. *Phys. Rev. Lett.*, 82:1526–9, 1999.

[57] B. Ludoph *et. al.* Evidence for saturation of channel transmission from conductance fluctuations in atomic-size point contacts. *Phys. Rev. Lett*, 82:1530–3, 1999.

[58] B. Ludoph and J.M. van Ruitenbeek. Thermopower of atomic-size metallic contacts. *Phys. Rev. B*, 59:12290–3, 1999.

[59] H. M. McConnell. Intromolecular charge transfer in aromatic free radicals. *J. Chem. Phys*, 35:508–516, 1961.

[60] N.D. Lang. Resistance of atomic wires. *Phys. Rev. B*, 52:5335–43.

[61] N.D. Lang. Resistance of a one-atom contact in the scanning tunneling microscope. *Phys. Rev. B*, 36:8173–6, 1987.

[62] N.D. Lang. Apparent barrier height in scanning tunneling microscopy. *Phys. Rev. B*, 37:10395–8, 1988.

[63] A. Yacoby N.D. Lang and Y.Imry. Theory of a single-atom point source for electrons. *Phys. Rev. Lett*, 63:1499–502, 1989.

[64] D. Turnbull F. Seitz and H. Ehrenreich (ed). *solid state physics, vol:28.* New York: Academic, 1973.

[65] N.D. Lang. Field-induced transfer of an atom between two closely spaced electrodes. *Phys. Rev. B*, 45:13599–606, 1992.

[66] M. Magoga and C. Joachim. Conductance and transparence of long molecular wires. *Phys. Rev. B*, 56:4722–29, 1997.

[67] M. Magoga and C. Joachim. Minimal attenuation for tunnelling through a molecular wire. *Phys. Rev. B*, 57:1820–3, 1998.

[68] M. Blencowe. Quantum energy flow in mesoscopic dielectric structures. *Phys. Rev. B*, 59:4992–8, 1999.

[69] P.A. Khomyakov and G. Brocks. Real-space finite-difference method for conductance calculations. *Phys. Rev. B*, 70:195402–15, 2004.

[70] P.A. Khomyakov *et. al.* Conductance calculations for quantum wires and interfaces: Mode matching and greenâĂŹs functions. *Phys. Rev. B*, 72:035450–63, 2005.

[71] J. Wang and J.S. Wang. Mode-dependent energy transmission across nanotube junctions calculated with a lattice dynamics approach. *Phys. Rev. B*, 74:054303–8, 2006.

[72] B. Hu P. Tong and B. Li. Wave transmission, phonon localization, and heat conduction of a one-dimensional frenkel-kontorova chain. *Phys. Rev. B*, 59:8639–45, 1999.

[73] L.S. Cao *et. al.* Delocalization of phonons and quantized thermal conductance in a random n -mer system. *Phys. Rev. B*, 72:214301–8, 2005.

[74] Y.M. Zhang and S.J. Xiong. Phonon transmission and thermal conductance in quasi-one-dimensional disordered systems. *Phys. Rev. B*, 72:115305–10, 2005.

[75] M.Kemp V. Mujica and M.A. Ratner. Electron conduction in molecular wires. i. a scattering formalism. *J. Chem. Phys*, 101:6849–55, 1994.

[76] M. Kemp V. Mujica and M.A. Ratner. Electron conduction in molecular wires. ii. application to scanning tunneling microscopy. *J. Chem. Phys.*, 101:6856–65, 1994.

[77] S.N. Yaliraki and M.A. Ratner. Molecule-interface coupling effects on electronic transport in molecular wires. *J. Chem. Phys.*, 109:5036–5044, 1998.

[78] C. Caroli *et. al.* Direct calculation of tunneling current. *J. Phys. C.*, 4:916–29, 1971.

[79] N.S. Wingreen *et. al.* Resonant tunneling with electron-phonon interaction: An exactly solvable model. *Phys. Rev. Lett.*, 61:1396–400, 1988.

[80] N.S. Wingreen *et. al.* Landauer formula for current through an interacting electron region. *Phys. Rev. Lett.*, 68:2512–7, 1992.

[81] N.S. Wingreen *et. al.* Time-dependent transport in interacting and non-interacting resonant tunneling regime. *Phys. Rev. B.*, 50:5528–48, 1994.

[82] N.S. Wingreen *et. al.* Inelastic scattering in resonant tunneling. *Phys. Rev. B.*, 40:11834–50, 1989.

[83] D. Sen and A. Dhar. Non-equilibrium green's function formalism and the problem of bound states. *Phys. Rev. B*, 73:085119–51, 2006.

[84] A.M. Kuznetsov and J. Ulstrup. *Electron Transfer in Chemistry and Biology: An Introduction to the theory.* Chichest:Wiley, 1999.

[85] A.M. Kuznetsov and J. Ulstrup. Mechanisms of in situ scanning tunnelling microscopy of organized redox molecular assemblies. *J. Phys. Chem. A*, 104:11531–50, 2000.

[86] A.M. Kuznetsov and W. Schmickler. Mediated electron exchange between an electrode and the tip of a scanning tunneling microscope âĂŞ a stochastic approach. *Chem. Phys*, 282:371–7, 2002.

[87] W. Schmickler. On the possibility of measuring the adsorbate density of states with a scanning tunneling microscope. *J. Electroanal. Chem*, 296:283–89, 1990.

[88] W. Schmickler and D. Henderson. A model for the scanning tunneling microscope operating in an electrolyte solution. *J. Electroanal. Chem*, 290:283–91, 1990.

[89] W. Schmickler and N.J. Tao. Measuring the inverted region of an electron transfer reaction with a scanning tunneling microscope. *Electrochim. Acta*, 432:2809–15, 1997.

[90] R. A. Marcus. Electron transfer reactions in chemistry, theory and experiment. *J. Electroanal. Chem*, 438:251–259, 1997.

[91] R. E. Goldstein S. Franzen and S. G. Boxer. Distance dependence of electron transfer reactions in organized systems: the role of superexchange and non-condon effects in photosynthetic reaction centers. *J. Phys. Chem*, 97:3040 – 3053, 1993.

[92] H. Sumi. Electron transfer via a midway molecule as seen in primary processes in photosynthesis: Superexchange or sequential, or unified? *J. Electroanal. Chem*, 438:11–20, 1997.

[93] C. Hsu. Application of sequential formula: the electronic coupling and the distance dependence in the electron transfer of ferrocene-terminated alkanethiol monolayers. *J. Electroanal. Chem*, 438:27 – 35, 1997.

[94] W. Knoll *et. al.* Supramolecular interfacial architectures for controlled electron transfer. *J. Electroanal. Chem*, 438:199 – 205, 1997.

[95] Y. Sato and F. Mizutani. Electrochemical responses of cytochrome c on a gold electrode modified with mixed monolayers of 3-mercaptopropionic acid and n-alkanethiol. *J. Electroanal. Chem*, 438:99 – 104, 1997.

[96] A. J. Bard *et. al.* The electrode/electrolyte interface - a status report. *J. Phys. Chem*, 97:7147 – 7173, 1993.

[97] S. Berchmans *et. al.* Solution phase electron transfer versus bridge mediated electron transfer across carboxylic acid terminated thiols. *J. Solid State Electrochem*, 10:439 – 446, 2006.

[98] Williams Rhain J. L. Daniel Bretts and C Paul Wilde. Temperature effects on the voltammetry of ferrocene terminated self-assembled monolayers. *J. Electroanal. Chem*, 65:538–539, 2002.

[99] M. T. Carter L. Tender and R. W. Murray. Cyclic voltammetry analysis of ferrocene alkanethiol monolayer electrode kinetics based on marcus theory. *Analytical Chem*, 66:3173 – 3181, 1994.

[100] K. Weber and S. E. Creager. Voltammetry of redox-active groups irreveribly adsorbed onto electrodes. treatement using the marcus relation between rate and overpotential. *Analytical Chemistry*, 66:3164 – 3172, 1994.

[101] H. O. Finklea A. J. Bard and I. Rubinstein (Eds). *Electroanalytical Chemistry vol-19*. Marcel Dekker: New York, 1996.

[102] L. H. Dubois and R. G. Nuzzo. Synthesis, structure, and properties of model organic structures. *Ann. Rev. Phys. Chem*, 43:437 – 463, 1992.

[103] J. Hudedeck S. D. More and T. Urisu. Hydrophobic/hydrophilic interactions of cytochrome c with functionalized self-assembled monolayers on silicon. *Surf. Sci*, 532:993 – 998, 2003.

[104] E. F. Bowden M. Collinson and M. J. Tarlov. Voltammetry of covalently immobilized cytochrome c on self-assembled monolayer electrodes. *langmuir*, 8:1247 – 1250, 1992.

[105] A. J. Bard Fu-Ren F. Fan. An electrochemical coulomb staircase: Detection of single electron-transfer events at nanometer electrodes, 1997.

[106] M. Ueda H. Nejoh and M. Aono. Single-electron-charging effect controlled by the distance between a substrate and a liquid-crystal molecule, 1993.

[107] S. Chen and K. Huang. Electrochemical and spectroscopic studies of nitrophenyl moieties immobilized on gold nanoparticles, 2000.

[108] L. Menon N. Kouklin and S. Bandyopadhyay. Room-temperature single-electron charging in electrochemically synthesized semiconductor quantum dot and wire array, 2002.

[109] D.M. Adams *et. al.* Charge transfer on the nanoscale: Current status. *J. Phys. Chem. B*, 107:6668–6697, 2003.

[110] C.S. Lent and P.D. Tougaw. A device architecture for computing with quantum dots. *Proc IEEE*, 97:541–557, 1997.

[111] I. Amlani *et. al.* Digital logic using quantum-dot cellular automata. *Science*, 284:289–91, 1999.

[112] R Kummamuru *et. al.* Power gain in a quantum-dot cellular latch. *App. Phys. Lett.*, 81:1332–4, 2002.

[113] M. Lieberman *et. al.* Quantum-dot cellular automata at a molecular scale. *Ann. N. Y. Acad. Sci.*, 960:225–29, 2002.

[114] M. T. Cygan *et. al.* Insertion, conductivity and structures of conjugated organic oligomers in self-assembled alkanethiol monolayer on au111. *J. Am. Chem. Soc*, 120:2721–2732, 1998.

[115] G. Decher. Fuzzy nanoassemblies: Toward layered polymeric multicomposites. *Science*, 277:1232–7, 1997.

[116] M. D. Newton. Quantum chemical probes of electron-transfer kinetics: the nature of donor-acceptor interactions. *Chem. Rev*, 91:767–92, 1991.

[117] W. B. Davis *et. al.* Electron transfer rates in bridged molecular systems: A phenomenological approach to relaxation. *J. Phys. Chem. A*, 91:6158–64, 1997.

[118] A. E. Roitberg V. Mujica and M. A. Ratner. Molecular wire conductance: Electrostatic potential spatial profile. *J. Chem. Phys*, 112:6834–9, 2000.

[119] G. Y. Hu and R. F. O'Connell. Quantum transport for a many-body system using a quantum langevin-equation approach. *Phys. Rev. B*, 36:5798–5808, 1987.

[120] S. Camalet *et. al.* Current noise in ac-driven nanoscale conductors. *Phys. Rev. Lett*, 90:210602–210606, 2003.

[121] S. Camalet *et. al.* Shot-noise control in ac-driven nanoscale conductors. *Phys. Rev. B*, 70:155326–155343, 2004.

[122] A. Nitzan D. Segal and P. Hänggi. Thermal conductance through molecular wires. *J. Chem. Phys*, 119:6840–6856, 2003.

[123] J. Taylor *et. al.* Ab initio modeling of quantum transport properties of molecular electronic devices. *Phys. Rev. B*, 63:245407–24520, 2001.

[124] J. Taylor *et. al.* Theory of rectification in tour wires: The role of electrode coupling. *Phys. Rev. Lett*, 89:138301–138305, 2002.

[125] S. T. Pantelides M. D. DiVentra and N. D. Lang. First-principles calculation of transport properties of a molecular device. *Phys. Rev. Lett*, 84:979–982, 2000.

[126] A. W. Ghosh P.S. Damle and S. Datta. unified description of molecular conduction: From molecules to metallic wires. *Phys. Rev. B*, 64:201403–201407, 2001.

[127] U. Lundin and H. McKenzie. Temperature dependence of polaronic transport through single molecules and quantum dots. *Phys. Rev. B*, 66:75303–75311.

[128] J. X. Zhu and A. V. Balatsky. Theory of current and shot-noise spectroscopy in single-molecular quantum dots with a phonon mode. *Phys. Rev. B*, 67:165326–165331, 2003.

[129] A. M. Bratkovsky A. S. Alexandrov and R. S. Williams. Bistable tunneling current through a molecular quantum dot. *Phys. Rev. B*, 67:075301–075305, 2003.

[130] A. S. Alexandrov and A. M. Bratkovsky. Memory effect in a molecular quantum dot with strong electron-vibron interaction. *Phys. Rev. B*, 67:235312–235320, 2003.

[131] K. Flensberg. Tunneling broadening of vibrational sidebands in molecular transistors. *Phys. Rev. B*, 68:205323–205330, 2003.

[132] M. B. Hastings D. Mozyrsky and I. Martin. Intermittent polaron dynamics: Born-oppenheimer approximation out of equilibrium. *Phys. Rev. B*, 73:035104–035110, 2006.

[133] W. Schmickler. On the possibility of measuring the adsorbate density of states with a scanning tunneling microscope. *J. Electroanal. Chem.*, 296:283–289, 1990.

[134] W. Schmickler and C. Widrig. The investigation of redox reactions with a scanning tunneling microscope: Experimental and theoretical aspects. *J. Electroanal. Chem.*, 336:213, 1992.

[135] P. Sommer-Larsen A. M. Kuznetsov and J. Ulstrup. Resonance and environmental fluctuation effects in stm currents through large adsorbed molecules. *Surf. Sci*, 275:52–64, 1992.

[136] W. Schmickler. Investigation of electrochemical electron transfer reactions with a scanning tunneling microscope: a theoretical study. *Surf. Sci*, 295:43–56, 1993.

[137] W. H. Han *et. al.* Stm contrast, electron-transfer chemistry and conduction in molecules. *J. Phys. Chem. B*, 101:10719–10725, 1997.

[138] R. E. Holmin *et. al.* Correlating electron transport and molecular structure in organic thin films. *Angew. Chem. Int. Edn*, 40:2316–2320, 2001.

[139] M. A. Rampi E. Tran and G. M. Whitesides. Electron transfer in hg-sam//sam-hg junction mediated by redox centers. *Angew. Chem. Int. Edn*, 43:3835–3839, 2004.

[140] T. Albrecht *et. al.* Scanning tunneling spectroscopy in an ionic liquid. *J. Am. Chem. Soc*, 128:6574–6575, 2006.

[141] Q. Chi *et. al.* Long-range interfacial electron transfer of metalloproteins based on molecular wiring assemblies. *Faraday Discuss.*, 131:181–197, 2006.

[142] Z. Li *et. al.* Two-dimensional assembly and local redox-activity of molecular hybrid structures in an electrochemical environoment. *Faraday Discuss.*, 131:121–145, 2006.

[143] S. Corni A. Alessandrini and P. Facci. Unravelling single metalloprotein electron transfer by scanning probe techniques. *Phys. Chem. Phys*, 8:4383–4397, 2006.

[144] T. Albrecht *et. al.* In situ scanning tunneling spectroscopy of inorganics transition metal complexes. *Faraday Discuss.*, 131:265–281, 2006.

[145] A. Nitzan M. Galperin and M. A. Ratner. The non-linear response of molecular junctions: the polaron model revisited. *J. Phys. Condens. Matter*, 20:374107–374113, 2008.

[146] A. M. Kuznetsov and I. G. Medvedev. A theory of redox-mediated electron tunneling through an electrochemical two-center contact. *J. Phys. Condens. Matter*, 20:374112–374113, 2008.

[147] W. Tian *et. al.* Conductance spectra of molecular wires. *J. Chem. Phys*, 109:2874–2883, 1998.

[148] J. Evenson and M. Karplus. Effective coupling in bridged elecctron transfer molecules: Computational formulation and examples. *J. Chem. Phys*, 96:5272–5279, 1992.

[149] W. Schmickler. Electron and ion transfer reactions on metal electrodes. *Electrochim. Acta*, 41:2329–2338, 1996.

[150] A. N. Kuznetsov and W. Schmickler. Mediated electron exchange between an electrode and the tip of scanning tunneling microscope - a stochastic approach. *Chem. Phys*, 282:371–377, 2002.

[151] A. M. Kuznetsov. *Charge Transfer in Physics, Chemistry and Biology.* Gordon and Breach, New York, 1995.

[152] A. Nozik R. J. Miller, G. McLendon and W. Schmickler. *Surface Charge Transfer Processes.* New York: VCH Publishers, 1995.

[153] W. Schmickler. *Interfacial Electrochemistry.* Oxford: Oxford University Press, 1996.

[154] R. Landauer. Spatial variations of currents and fields due to localized scatterers in metallic conduction. *IBM. J. Res. Dev*, 1:223–228, 1957.

[155] M. Buttiker. Four-terminal phase-coherent conductance. *Phys. Rev. Lett*, 57:1761–1764, 1986.

[156] M. Buttiker. Coherent and sequential tunneling in series barriers. *IBM. J. Res. Dev*, 32:63–75, 1988.

[157] Y. Imry. *Introduction to Mesoscopic Physics.* Oxford: Oxford University Press, 1997.

[158] J. L. D' Amato and H. M. Pastawski. Conductance of a disordered linear chain including inelastic scattering events. *Phys. Rev. B*, 41:7411–7420, 1990.

[159] D. Segal *et. al.* Electron transfer rates in bridged molecular systems 2.a steady-state analysis of coherent tunneling and thermal transitions. *J. Phys. Chem. B*, 104:3817–3829, 2000.

[160] J. W. Evenson and M. J. Karplus. Effective coupling in biological electron transfer: exponential or complex distance dependence? *science*, 262:124–1249, 1993.

[161] C. P. Hsu and R. A. Marcus. A sequential formula for electronic couping in long range bridge-assisted electron transfer: Formulation of theory and application to alkanethiol monolayers. *J. Chem. Phys*, 106:584–599, 1997.

[162] J. Betts D. N. Beratan and J. N. Onuchic. Protein electron transfer rates set by the bridging secondary and tertiary structure. *Science*, 252:1285–1288, 1991.

[163] A. A. Stuchebrukhov. Tunneling currents in electron transfer reactions in proteins. *J. Chem. Phys*, 104:8424–8433, 1996.

[164] C. Goldman. Long-range electron transfer in proteins: A renormalized-perturbation-expansion approach. *Phys. Rev. A*, 43:4500–4509, 1991.

[165] E. S. Medvedev and A. A. Stuchebrukhov. Inelastic tunneling in long-distance biological electron transfer reactions. *J. Chem. Phys*, 107:3821–3832, 1997.

[166] W. T. Pollard A. K. Felts and R. A. Friesner. Multilevel redfield treatment of bridge-mediated long-range electron transfer: A mechanism for anamalous distance dependence. *J. Phys. Chem*, 99:2929–2940, 1995.

[167] W. T. Pollard A. K. Felts and R. A. Friesner. The redfield equation in condensed-phase quantum dynamics. *Adv. Chem. Phys.*, 93:77, 1996.

[168] V. Chernyak A. Okada and S. Mukamel. Solvent reorganization in long-range electron transfer: Density matrix approach. *J. Phys. Chem. A.*, 102:1241–1251, 1998.

[169] S. S. Skourtis and S. Mukamel. Superexchange versus sequential long range electron transfer; density matrix pathways in liouville space. *Chem. Phys*, 197:367–388, 1995.

[170] Y. Tanimura and P. G. Wolynes. Quantum and classical fokker-planck equations for a gaussian-markovian noise bath. *Phys. Rev. A*, 43:4131–4242, 1991.

[171] Y. Tanimura and P. G. Wolynes. The interplay of tunneling, resonance, and dissipation in quantum barrier crossing: A numerical study. *J. Chem. Phys*, 96:8485–8497, 1992.

[172] R. A. Drust *et. al.* Chemically modified electrodes: Recommended terminology and definitions. *Pure and Appl. chem*, 69:1317–24, 1997.

[173] T. Xu R. M. Metzger and I. R. Peterson. Electrical rectification by a monolayer of hexadecylquinolinium tricyanoquinodimethanide measured between macroscopic gold electrodes. *J. Chem. Phys. B*, 105:7280 – 90, 2001.

[174] A. Salomon *et. al.* Comparison of electronic transport measurements on organic molecules. *Adv. Mater*, 15:1881 –90, 2003.

[175] J. Jortner and M. Bixon. *Electron Transfer from Isolated Molecules to Biomolecules.* Wiley: New York, 1999.

[176] A. Muller. *Electron and Proton Transfer in Chemistry and Biology.* Elsevier: Amsterdam, 1992.

[177] M. A. Reed *et. al.* Conductance of molecular junction. *Science*, 278:252 –4, 1997.

[178] C. Joachim *et. al.* Electronic transparence of a single c_{60} molecule. *Phys. Rev. Lett*, 74:2102 – 5, 1995.

[179] F. Remacle and R. D. Levine. Electrical transport in saturated and conjugated molecular wires. *Faraday Discussion*, 131:45 – 67, 2006.

[180] S. M. Lindsay. Molecular wires and devices: Advances and issues. *Faraday Discussion*, 131:403 –11, 2006.

[181] C. Joachim and S. Roth. *Atomic and Molecular wires.* Kluwer acdemic: Dordrecht, 1997.

[182] A. K. Mishra. Electronic structure of a chemisorbed layer at electrochemical interface: Copper layer on gold electrode. *J. Phys. Chem. B*, 103:1484 – 98, 1999.

[183] A. K. Mishra R. Kishore and W. Schmickler. Metal - insulator transition in a layer adsorbed on a metal electrode. *J. Electroanal. Chem*, 574:1 –, 2004.

[184] A. K. Mishra and W. Schmickler. Potential energy surface for an electron transfer reaction mediate by a metal adlayer. *J. Chem. Phys*, 121:1020 –9, 2004.

[185] A. Tadjeddine *et. al.* Electronic and structural characterization of underpotentially deposited submonolayers and monolayers of copper on gold (111) studies by *in situ* x-ray absorption spectroscopy. *Phys. Rev. Lett*, 66:2235 – 8, 1991.

[186] J. Neugebauer and M. Scheffler. Adsorbate-substrate and adsorbate-adsorbate interactions of na and k adlayers on al(111). *Phys. Rev. B*, 46:16067 – 80, 1992.

[187] J. Neugebauer and M. Scheffler. Mechanism of island formation of alkali-metal adsorbates on al(111). *Phys. Rev. Lett*, 71:577 – 80, 1993.

[188] H. Over *et. al.* Structural properties of alkali-metal atoms adsorbed on ru(0001). *Surf. Rev. Lett*, 2:409 – 22, 1995.

[189] A. K. Mishra and S. K. Rangarajan. Two-adsorbate problem: a superoperator analysis. *J. Phys. Chem*, 91:3406 –16, 1987.

[190] W. Schmickler. A model for electron transfer reactions via adsorbed intermediates. *J. Electroanal. Chem*, 113:159 – 170, 1980.